CFAP61 is required for sperm flagellum formation and male fertility in human and mouse

Siyu Liu[1#], Jintao Zhang[1#], Zine Eddine Kherraf[2,3], Shuya Sun[1], Xin Zhang[1], Caroline Cazin[2,3], Charles Coutton[2,4], Raoudha Zouari[5], Shuqin Zhao[6], Fan Hu[7], Selima Fourati Ben Mustapha[5], Christophe Arnoult[2], Pierre F Ray[2,3*], Mingxi Liu[1*]

1 State Key Laboratory of Reproductive Medicine, Department of Histology and Embryology, School of Basic Medical Sciences, Nanjing Medical University, Nanjing, 211166, China
2 Univ. Grenoble Alpes, INSERM U1209, CNRS UMR 5309, Institute for Advanced Biosciences, Team Genetics Epigenetics and Therapies of Infertility, Grenoble, F-38000, France
3 CHU de Grenoble, UM GI-DPI, Grenoble, F-38000, France
4 CHU de Grenoble, UM de Génétique Chromosomique, Grenoble, F-38000, France
5 Polyclinique les Jasmins, Centre d'Aide Médicale à la Procréation, Centre Urbain Nord, Tunis, Tunisia
6 State Key Laboratory of Reproductive Medicine, Animal Core Facility of Nanjing Medical University, Nanjing 211166, China
7 State Key Laboratory of Reproductive Medicine, Nanjing Medical University, Nanjing, 211166, China

[#]Contributed equally to this work.
*Corresponding authors:
Mingxi Liu: mingxi.liu@njmu.edu.cn
Pierre F. Ray, E-mail address: pray@chu-grenoble.fr

Keywords：cilia/flagella；MMAF；spermatogenesis；male infertility; radial spoke；CSC

Summary statement

We demonstrated that CFAP61, as a component of radial spoke and CSC, is crucial for spermatogenesis.

Abstract

Defects in the structure or motility of cilia and flagella may lead to severe diseases such as primary ciliary dyskinesia (PCD), a multisystemic disorder with heterogeneous manifestations affecting primarily respiratory and reproductive functions. We report that CFAP61 is a conserved component of the Calmodulin and radial Spoke associated Complex (CSC) of cilia. We find that a *CFAP61* splice variant, c.143+5G>A, causes exon skipping/ intron retention in human, inducing a multiple morphological abnormalities of the flagella (MMAF) phenotype. We generated *Cfap61* knockout mice that recapitulate the infertility phenotype of the human *CFAP61* mutation, but without other symptoms usually observed in PCD. We find that CFAP61 interacts with the CSC, radial spoke (RS) stalk and head. During early stages of *Cfap61*$^{-/-}$ spermatid development, the assembly of RS components is impaired. With the progress of spermiogenesis, the axoneme in *Cfap61*$^{-/-}$ cells becomes unstable and scatters, and the distribution of intraflagellar transport proteins is disrupted. This study reveals an organ specific mechanism of axoneme stabilization that is related to male infertility.

Introduction

Motile cilia and flagella are highly conserved cell organelles, they present a similar structure organized around a microtubule-based cytoskeleton called the axoneme but differ in length and functions. In mammals, defects in cilia lead to severe diseases, mainly primary ciliary dyskinesia (PCD) which affects approximately 1:10,000 individuals worldwide (Lucas et al., 2014, Rubbo and Lucas, 2017). PCD is a multisystemic disorder caused by motility defects of cilia and flagella (Afzelius and Eliasson, 1983, Munro et al., 1994), mainly characterized by recurrent respiratory tract infections with varying symptoms ranging from chronic rhinosinusitis to bronchiectasis and male infertility due to sperm immotility (Ibanez-Tallon et al., 2003). Female subfertility is less common and is caused by dysmotile fallopian tube cilia (Lyons et al., 2006). In 50% of cases, PCD is also associated with situs inversus, due to dysfunction of motile embryonic node cilia perturbing organ laterality (Coutton et al., 2015). More rarely, hydrocephalus arises as a consequence of ependymal cilia dysmotility leading to a blockage of the cerebrospinal fluid flow (Lyons et al., 2006). The gross axonemal structure of motile cilium and sperm tail may appear identical, but there are cell type-specific differences in axonemal proteins such as dynein arm components and in the assembly of the axoneme (Fliegauf et al., 2007). This is supported by the fact that basic motility and morphological aspects differ between motile cilia and sperm and also that not all

mutations in PCD genes cause male infertility, such as *CCDC114* (Onoufriadis et al., 2013) and *RSPH4A* (Moryan et al., 1985). Conversely, many axonemal genes have been described to induce male infertility without any other PCD symptoms, as exemplified by *DNAH1*, which, when mutated, leads to a male infertility phenotype characterized by multiple morphological abnormalities of the flagella (MMAF) (Ben Khelifa et al., 2014). Since the first report of this severe flagellar defect in 1984, this rare phenotype has been subsequently described as 'dysplasia of the fibrous sheath', 'short tails' or 'stump tails' , and this heterogeneous group of flagellar defects was named 'MMAF' for multiple morphological anomalies of the flagella to standardise all these terms (Coutton et al., 2015). Exome sequencing allowed researchers to partially elucidate genetic and physiopathological mechanisms that lead to sperm flagellum defects and, to date, variants in at least 20 genes have been found to be associated with the MMAF phenotype (Ben Khelifa et al., 2014, Beurois et al., 2019, Coutton et al., 2019, He et al., 2019, He et al., 2020, Liu et al., 2019a, Liu et al., 2019b, Liu et al., 2019c, Liu et al., 2020, Li et al., 2020, Lorès et al., 2018, Lv et al., 2020, Martinez et al., 2018, Sha et al., 2017, Shen et al., 2019, Tang et al., 2017, Auguste et al., 2018, Li et al., 2019, Martinez et al., 2020, Kherraf et al., 2018, Zhang et al., 2021).

In mammals, flagella are essential for male gamete motility. The axoneme is the main component of the flagellum and runs through its entire length including the neck, middle, principle and end segments (Lindemann and Lesich, 2016). The axoneme has been extensively studied, mainly in flagella/ciliated unicellular organisms and sea urchin sperm, describing a structure conserved from single-celled protists to mammals. This core structure contains a central pair (CP) of singlet microtubules (MTs) surrounded by nine outer MT doublets. Each doublet contains a sequence of identical building blocks, which repeat longitudinally every 96 nm. Neighboring doublets are interconnected circumferentially by nexin links and are attached to the CP through radial spokes (RSs). The dynein motors responsible for motility are organized into two rows of outer and inner arms along the length of the doublets. Dyneins are minus end–directed motors, and their unidirectional movement along a B-tubule induces bending in one direction, whereas the dyneins located on the opposite side of the axoneme induce bending to the opposite direction (Heuser et al., 2012). Structures important for the coordination of dynein activity include the CP complex, the RSs, the I1 inner arm dynein, and the dynein regulatory complex (DRC) (Lorès et al., 2018, Coutton et al., 2018, Dong et al., 2018, Sha et al., 2017, Kherraf et al., 2018).

Björn Afzelius, in 1959, was the first to describe the presence of RSs in the axonemes of sea urchin sperm flagella (Satir, 1968). In addition to their structural role in maintaining the 9+2 axoneme stability, RSs seem to also be involved in the beating motion, participating in signal transduction between the CP and the dyneins (Abbasi et al., 2018, Shinohara et al., 2015, Liu et al., 2020). Initially, SDS‐PAGE analysis of axonemes of wild-type (WT) and paralyzed mutants of *Chlamydomonas* revealed 17 polypeptide chains that were ascribed to the RS complex (Piperno et al., 1981, Whitfield et al., 2019), and the eventual purification of the RS complex (Beurois et al., 2019, Li et al., 2020) enabled the identification of 23 proteins (Beurois et al., 2019, Martinez et al., 2020). These proteins were called RSP1 to RSP23, and in *Chlamydomonas* the RSPs (1–12, 14, 16-17, 20, 22 and 23) have been identified and sequenced (Yang et al., 2004, Williams et al., 1989, Curry et al., 1992, Yang et al., 2005, Zimmer et al., 1988, King and Patel-King, 1995, Patel-King et al., 2004, Yang et al., 2006). RSPs are assembled into RSs in two phases. Separation of the RSPs on sucrose density gradients permitted to identify and characterize different S(ucroses) fractions/particles. First, the cell assembles partial RSs as 12S particles, composed of RSPs 1-7 and 9-12 (Diener et al., 2011, Pigino et al., 2011, Qin et al., 2004). After delivery to the flagella by intraflagellar transport (IFT), 12S precursors are converted into 20S mature RSs, by the assembly of the remaining RSPs (Diener et al., 2011, Pigino et al., 2011). Regarding these later assembled RSPs, the knowledge on RSPs 13, 15, 18, 19, 21 is still relatively limited, but interestingly, in subsequent studies, RSP18 and RSP19 were found to be involved in the calmodulin (CaM)- and spoke-associated complex (CSC). Both RSP18 and RSP19 are present in axonemes from *pf14*, a *Chlamydomonas* radial spoke mutant that lacks radial spoke structure (Piperno et al., 1981). In a recent report, lack of *Cfap61* in mice resulted in an MMAF phenotype and male sterility (Huang et al., 2020). The precise mechanism by which CFAP61 regulates sperm flagella formation in mammals is still unclear.

In the present study, we found that a splice-site variant c.143+5G>A of the *RSP19* homologous gene, *CFAP61*, leads to exon skipping/ intron retention and induces MMAF in humans. In addition, CFAP61 has been found to interact with the CSC, RS stalk and RS head. In the early stages of *Cfap61*$^{-/-}$ spermatid development, RS 12S precursors were assembled, but the assembly of other RS components was blocked, and with the progress of spermiogenesis, the axoneme became unstable and was severely altered in *Cfap61* knockout mice. This defect was only observed in the assembly of the flagellum axoneme, while there was no effect on cilia. In addition, the absence of *Cfap61* also affected the distribution of IFT

in the sperm flagellum. Therefore, this study reveals an organ dependent mechanism of axoneme stabilization that is related to male infertility.

Results

Cfap61 is an evolutionarily conserved gene predominantly expressed in the testis

In *Chlamydomonas*, the CSC is located at the base of RS and interacts with the DRC and inner dynein arm (IDA) (Dymek and Smith, 2007, Heuser et al., 2012, Urbanska et al., 2015, Viswanadha et al., 2017) (Fig. 1A), while CaM interacting proteins, CaM-IP1-3 (FAP91, FAP61 and FAP251), are considered components of the CSC (Heuser et al., 2012). Mutations in the human homologues, *MAATS1* (*FAP91* homologous gene) (Martinez et al., 2020) and *CFAP251* (*FAP251* homologous gene) (Auguste et al., 2018, Kherraf et al., 2018, Li et al., 2019) have been detected in patients with MMAF. We evaluated the expression of potential CSC components in various organs in mice and found that CSC components were predominantly expressed in the testis (Fig. 1B,C,D). The *FAP61* homologous gene, *Cfap61*, was detectable in testis, brain and lung, but its testis expression level was much higher than that in other organs (Fig. 1B). *Maats1* (*FAP91* homologous gene) and *Wdr66* (*FAP251* homologous gene) showed similar expression patterns in mice (Fig. 1C,D). Regarding the components of RS, we observed a distinct expression pattern in different organs. For example, *Armc4 (Rsph8)* and *Rsph9* are preferentially expressed in the testis, while *Rsph4a* is highly expressed in the lung (Fig. 1E,F,G). Among basal eukaryotes, *Cfap61* is expressed in species that present a flagellum at some stage of the organism's life cycle. The CFAP61 protein is composed of a domain of unknown function (DUF4821) and protein sequence alignment showed that CFAP61 is an evolutionarily conserved gene present among human, mouse, rat, Xenopus, zebrafish and *Chlamydomonas* (Fig. 1H).

Exome sequencing identified *CFAP61* homozygous variants in patients with MMAF

A cohort of 167 patients with MMAF and no other signs of PCD was previously analyzed and permitted to identify harmful variants in known MMAF-related genes in 66 patients (Martinez et al., 2020). After reanalysis of the exomes data from the undiagnosed subjects, we identified one patient with a homozygous variant in *CFAP61*. This patient (PaCFAP61) had an intronic variant predicted to alter splicing: c.143+5G>A (NM_015585.4) (Fig. 2A). The variant was present in the Genome Aggregation Database with a minor allele frequency of 1.59e-5. Additionally, we found by minigene assay that c.143+5G>A induced the skipping of *CFAP61* exon 2 and induced a frame-shift shortly after exon1 (Fig. 2B,C). In

order to further study the effects of c.143+5G>A mutation on RNA splicing and protein expression, all exons including upstream and downstream intronic sequences of exon2 were cloned into the pCAG1.1-3xFlag vector (Fig. 2D). Using RT-PCR and Sanger sequencing, we found skipping of exon 2 and the retention of intron 2 induced by c.143+5G>A mutation (Fig. 2E,F). Western blot analysis confirmed the expression of aberrant CFAP61 in HEK293T cells transfected with pCAG1.1-CFAP61-3xFlag plasmid carrying c.143+5G>A mutation (Fig. 2G).

These results suggest that c.143+5G>A affects the normal function of CFAP61 in humans and leads to MMAF. PaCFAP61 presented a typical MMAF phenotype with a semen volume of 3ml, 40M of sperm/ml, 20% of progressive motility and multiple flagellar anomalies: 36% of bent, 18% with no tail, 12% with a short tail, 50% with an irregular shape and 30% with a coiled tail.

CFAP61 is a component of sperm flagella CSC and radial spoke

We next performed immunoprecipitation (IP)-mass spectrometry of CFAP61 to determine the CFAP61 interactome in mouse testis (Fig. S1A). We found that the proteins interacting with CFAP61 include axonemal components and involved in its functional regulation and assembly (Fig. S1B). Through co-IP, we confirmed that murine CFAP61 interacts with MAATS1 from CSC (Fig. 3A,B). CFAP61 can also interact with RS stalk proteins, such as ARMC4 (RSPH8), RSPH3A and ROPN1/ROPN1L (RSPH11) (Fig. 3C,D,E,F). A RSP22 homologous protein, DYNLL2, was detected in interaction with CFAP61 by mass spectrometry (Fig. S1B), but co-IP results showed that CFAP61 and DYNLL2 (RSPH22) had no direct interaction with each other (Fig. S2B). These results suggest that any interaction between CFAP61 and DYNLL2 in the testis would be indirect.

Since previous reports have suggested that CFAP61 is a CSC component (Dymek and Smith, 2007, Heuser et al., 2012, Urbanska et al., 2015), an interaction between CFAP61 and the RS stalk can be predicted. Surprisingly, both our mass spectrometry data and co-IP data showed that CFAP61 can also interact with RSPH9, the RS head component (Fig. S1B and Fig. 3G,M). Futhermore, we used the Proximity Ligation Assay (PLA), which allows the detection of the close proximity between two protein within cells (less than 40nm) (Söderberg et al., 2006). Using both CFAP61 and RSPH9 antibodies, PLA revealed a characteristic dotted pattern throughout the flagella of spermatozoa (Fig. 3N). Similar to data in mice, the co-IP assay showed that *Chlamydomonas* FAP61 also interacted directly with FAP91, RSP8, RSP3, RSP11 and RSP9 (Fig. 3H,I,J,K,L), but not with RSP22 (Fig. S2A). In

addition, we found that CFAP61 could interact with DYNCLI2 and DYNLT1A of the dynein arm and TUBB3 (Fig. S2C,D,E). In *Chlamydomonas*, the dynein arm IA4 (dynein E) is greatly reduced in all CSC mutants (Heuser et al., 2012). These results suggest that CSC interaction with the dynein arms is conserved among species.

Besides, we also evidenced a close proximity between CFAP61 and CSNK2A2 by PLA (Fig. S1C, upper panel). Similar phenomenon also exists between CFAP61 and PPP1CC (Fig. S1C, lower panel). Although the significance of the interactions is still unknown, it is worth noted that *Ppp1cc* knockout can cause sperm tail deformity and dyskinesia (Sinha et al., 2013), while *Csnk2a2* knockout mice can also cause sperm deformity (Xu et al., 1999).

Deletion of CFAP61 resulted in abnormal sperm flagella RS, but did not affect the structure and function of respiratory cilia.

In order to investigate whether CFAP61 deletion affects the assembly of RS. We generated a *Cfap61* mutant mouse strain using the CRISPR/Cas9 system. A stable *Cfap61* mutant mouse line carrying two allelic variants: a 1-bp and 10-bp deletion within exon4 (Fig. S3A) was established and male mice homozygous for this allele are referred herein as *Cfap61*$^{-/-}$. Two mouse CFAP61 peptides were selected as antigens to generate specific antibodies (Fig. S4), western blot and immunofluorescence confirmed that CFAP61 was completely erased in *Cfap61*$^{-/-}$ testis (Fig. S3B,C). In testicular histological sections, CFAP61 was mainly distributed in the spermatozoa in seminiferous tubules from wild-type mice (Fig. S3C). *Cfap61*$^{-/-}$ males show no overt abnormality in development or behavior. To test male fertility, individual males (*Cfap61*$^{+/+}$ and *Cfap61*$^{-/-}$) were housed with *Cfap61*$^{+/+}$ (wild-type) females and the number of pups per litter was recorded. *Cfap61*$^{-/-}$ males failed to sire any offspring despite copulating with females (Fig. S3D). Gross examination of testis revealed no difference in appearance and testis weight between *Cfap61*$^{+/+}$ and *Cfap61*$^{-/-}$ littermates (Fig. S3E,F). Using Periodic acid–Schiff (PAS) staining, we found that *Cfap61*$^{-/-}$ lacked flagella with normal length in the lumen of seminiferous tubules (Fig. S5A,B). Western blot analysis showed that CFAP61 was mainly expressed in the testis among ciliated/flagellated organs (Fig. 4A) and protein extracts from sperm revealed that CFAP61 is in a Triton-resistant, SDS-soluble pool (Fig. 4B). Confocal microscopy reveals CFAP61 expression along the flagella in mouse spermatids (Fig. 4C,D,E,F,G,H,I,J,K,L,M,N).

When examining epididymis sections, *Cfap61*$^{-/-}$ seemed to contain less spermatozoa in the cauda and caput regions than *Cfap61*$^{+/+}$ mice (Fig. S5C,D,E,F), which was confirmed by the number of sperm collected from epididymal cauda of knockout mice that was significantly lower than in wild-type mice (Fig. 5A). Almost all *Cfap61*$^{-/-}$ spermatozoa were abnormal and showed short, bent, curled, thick or missing flagella (Fig. S6). Similar phenotypes were reported in a contemporaneous study of another *Cfap61* knockout mouse(Huang et al., 2020). The acrosome morphology of *Cfap61*$^{-/-}$ sperm was normal, while the formation of the tail was clearly disordered (Fig. 5B,C,D,E,F). These severe tail deformities of *Cfap61*$^{-/-}$ sperm have great influence on sperm movement. *Cfap61*$^{-/-}$ sperm showed a state of immobility (Movies 1,2). Base on *Cfap61*$^{-/-}$ mice, we used confocal microscopy to access the expression of RSPH9 and NME5 (RSPH23) proteins in sperm. Both RSPH9 and NME5 signals were very low in *Cfap61*$^{-/-}$ spermatozoa (Fig. 6).

To investigate if *Cfap61*$^{-/-}$ mice recapitulated the respiratory phenotype observed in PCD, we evaluated the distribution of RS proteins in tracheal cilia. Immunofluorescence signals of RSPH9 and NME5 in trachea cilia were evaluated by high resolution microscopy, and no difference was observed between *Cfap61*$^{-/-}$ and *Cfap61*$^{+/+}$ mice (Fig. 7A,B). Additionally, no expression of CFAP61 was detected in the respiratory tract cilia in both *Cfap61*$^{-/-}$ and *Cfap61*$^{+/+}$mice(Fig. 7A,B), which is consistant with the western blot results (Fig. 4A). Scanning electron microscopy did not detect any significant change in the length of respiratory tract cilia in *Cfap61*$^{-/-}$ mice (Fig. 7C,D,E,F). Similarly, there was no difference in the beating of trachea cilia from *Cfap61*$^{-/-}$ and *Cfap61*$^{+/+}$ animals (Movies 3, 4). These results suggest that CFAP61 plays an essential role in the formation of the RS structure in mammalian sperm flagellum, but is not necessary for respiratory cilia.

The absence of *Cfap61* leads to flagella axoneme assembly failure and sperm deformation

In order to understand the role of CFAP61 for flagellum assembly, we analyzed flagellum formation during spermiogenesis (Fig. 8A) and found that in *Cfap61*$^{-/-}$ mice, axonemes formed normally until the step 2 of spermatid formation (Fig. 8A, lower pannel). However, with the progress of spermatid differentiation, the microtubule structure became disordered and could not form a normal axonemal structure (Fig. 8A, lower pannel). Using transmission electron microscopy, we observed that *Cfap61*$^{-/-}$ microtubules and outer dense fibers were separated from the axoneme (Fig. 8B,C); however, centriole anchoring and implantation fossa formation were not affected (Fig. 8D). We further assessed the assembly of RS

components during spermiogenesis. In the axoneme of *Chlamydomonas*, the 12S RS complex as a whole is assembled first, and the other RS components, such as RSP23 and RSP16, are assembled later as the 20S RS complex (Diener et al., 2011, Pigino et al., 2011). In mice, we found that the assembly of RSPH9 in round spermatids was normal (Fig. 9A,B,C,D), but was missing in elongating spermatids of *Cfap61* knockout mice (Fig. 9E,F,G,H,I,J). In addition, we show that the non-12S RS component, NME5 (RSPH23), failed to assemble in *Cfap61*$^{-/-}$ round and elongating spermatids (Fig. 9K,L,M,N,O,P,Q,R,S,T). With the genesis of sperm morphological deformation, the axoneme become unstable and completely scattered. This suggests that CFAP61 plays an irreplaceable role in the assembly of the 20S RS complex in mammalian flagella and indicates that incomplete assembly of 20S RS component does not allow RS stability. In the late stages of spermatid flagellum assembly, the assembled 12S RS proteins seem to disappear from the flagellum due to the absence of CFAP61. Interestingly, there was no RS assembly abnormality in *Cfap61*$^{-/-}$ respiratory cilia, suggesting that *Cfap61* function is limited to sperm flagellum in mammals.

Through co-immunoprecipitation, we demonstrate that CFAP61 can interact with intraflagellar transport (IFT) components in vitro, such as WDR35, IFT22 and IFT81 (Fig. S7A,B,C). Furthermore, results of co-IP analysis indicated that CFAP61 bound IFT81 directly in vivo (Fig. S7D). IP-mass spectrometry showed that CFAP61 and IFT74 may interact indirectly, as IFT74 is a component of the IFT-B subcomplex (Lechtreck, 2015). Immunofluorescence showed that the IFT74 structure was located in the axoneme at the early stage of flagellum assembly, but not in the axoneme of elongating spermatid, when it was mainly located in the manchette (Fig. S7E,F,G). Similar to IFT74, CFAP61 is also located in the manchette of the elongating spermatid (Fig. 4I,J,K). In *Cfap61*$^{-/-}$ spermatids, no changes were observed in IFT proteins in the early stage of spermiogenesis, but they appeared to be trapped in the flagellum of the elongating spermatid (Fig. S7H,I,J,K,L). Although we are not sure whether this IFT retention is another cause for the abnormal flagellum assembly, it shows that the absence of *Cfap61* has a variety of effects on flagellum formation.

Discussion

In the present study, we describe a novel *CFAP61* variant c.143+5G>A inducing exon skipping and participating in the pathogenesis of MMAF. In *Chlamydomonas*, the CFAP61 homologous protein FAP61 was initially detected in the 20S RS complex (Beurois et al., 2019, Martinez et al., 2020), but in later studies FAP61 was found to remain in RS1 and RS2 deleted flagella. Meanwhile, FAP61 can interact with CaM, suggesting that it may be a CSC

component (Dymek and Smith, 2007, Heuser et al., 2012, Urbanska et al., 2015). Our study found that CFAP61 is a CSC component and also a RS component, and that CFAP61 can interact with CSC components and with ARMC4 (RSPH8), RSPH3, AROPN1/ROPN1L (RSPH11) and RSPH9 of the RS complex. These interactions also exist in *Chlamydomonas* homologous proteins. Although we do not have crystallographic evidence or single-particle cryo-electron microscopy data to confirm the molecular structure of CFAP61, our interactome data allow for an estimate of the position of CFAP61 in RS and CSC.

Dynein arms, DRC and RS regulate sperm motility (Viswanadha et al., 2017). Interestingly, deficiency of dynein arms, DRC or RS affect the length of the flagella and the assembly of microtubules and appendages in different degrees in spermatozoa (Ben Khelifa et al., 2014, Dutcher et al., 2020, Abbasi et al., 2018). The reasons behind this phenotype are not clear, but we observed that these abnormalities may be independent of motility regulation. For example, as a DRC component, *Tcte1* deletion affects sperm motility, but has little effect on sperm tail morphology (Castaneda et al., 2017). Here, axonemes from *Cfap61*$^{-/-}$ early round spermatids, appeared normal, however their structure became disordered in elongating spermatids and spermatozoa, but the positioning of the centrioles and of the implantation fossa formation were not affected. This abnormal phenomenon of spindle wire assembly cannot be explained only by the known functions of RS or CSC. In the early spermatids stage, the 12S RS complex contributes to form the axoneme, but is eliminated in *Cfap61*$^{-/-}$ elongating spermatid. These results suggest that CFAP61, is an important protein in the late stages of RS assembly and is necessary for the structural stability of the flagellum.

We observed that other proteins that interact with CFAP61 may also be involved in the assembly process of the flagellum and that IFT proteins were retained in the flagellum in *Cfap61*$^{-/-}$ elongating spermatids. The reason for IFT retention is still not clear, but may be due to the disorganization of the axoneme or could mean that the absence of CFAP61 has a direct effect on the IFT movement. However, no abnormal axoneme assembly was observed in the cilia of respiratory tract cells, suggesting that CFAP61 is not essential in these cells or that a stricter checkpoint mechanism may exist in the process of spermatozoa flagellum formation. In addition, we found that CFAP61 interacts with a large number of phosphorylation related proteins, although the specific functions and subcellular localization of these proteins are still unclear and need to be further studied.

In conclusion, we described significant differences in the assembly and structural stability of the axoneme in *Cfap61*$^{-/-}$ flagellum and cilia. Therefore, *Cfap61* has a unique function in the process of flagellum formation. These results provide a theoretical basis for differential regulation of cilia/flagellum formation and MMAF physiopathology.

Materials and Methods

Study Patients

Here, we re-analyzed our data obtained by WES performed for a total of 167 individuals affected by primary infertility associated with a MMAF and described previously(Coutton et al., 2019, Liu et al., 2020). We focused the analyses on patients for whom no genetic diagnosis had been reached. All the recruited subjects displayed isolated infertility with no other clinical features; in particular, primary ciliary dyskinesia (PCD) syndrome was excluded. All individuals presented with a typical MMAF phenotype, which is characterized by severe asthenozoospermia (total sperm motility below 10%; normal values 40%) with at least three of the following flagellar abnormalities present in >5% of the spermatozoa: short, absent, coiled, bent, or irregular flagella. All individuals had a normal somatic karyotype (46, XY) with normal bilateral testicular size, hormone levels, and secondary sexual characteristics. Informed consent was obtained from all the individuals participating in the study according to local protocols and the principles of the Declaration of Helsinki. The study was approved by local ethics committees, and samples were then stored in the CRB Germethèque (certification under ISO-9001 and NF-S 96-900) according to a standardized procedure or were part of the Fertithèque collection declared to the French Ministry of health (DC-2015-2580) and the French Data Protection Authority (DR-2016-392).

Whole exome sequencing (WES)

Genomic DNA was isolated from EDTA blood using the DNeasy Blood & Tissue Kits from QIAGEN SA (Courtaboeuf, France) or from saliva using the Oragen DNA extraction kit (DNAgenotech®, Ottawa, Canada) or from saliva using the Oragen DNA extraction kit (DNAgenotech®, Ottawa, Canada). Coding regions and intron/exon boundaries were sequenced on the Novogen platform (agilent v6, HiSeqX,) after enrichment with Agilent kits (Agilent Technologies, Wokingham, UK). Exomes data were analysed using a bioinformatics pipeline developed in-house using two modules, both distributed under the GNU General Public License v3.0 and available on github: https://github.com/ntm/grexome-TIMC-Primary and https://github.com/ntm/grexome-TIMC-Secondary and as described in part in

reference(Arafah et al., 2020). Variants with a minor allele frequency greater than 1% in gnomAD v2.0, 3% in 1,000 Genomes Project phase 3, or 5% in NHLBI ESP6500, were filtered out and only variants predicted to have high-impact (e.g. stop-gain or frameshift variants) by variant Effect Predictor v92 (McLaren et al., 2016) were scrutinized.

Animals

All mice used in this study were housed in a controlled environment at 20–22°C with a 12h light/dark cycle, 50–70% humidity, food and water *ad libitum*. All studies were approved by the Institutional Animal Care and Use Committees of Nanjing Medical University (Approval No. IACUC-1810020), Nanjing, China. All experiments with mice were conducted ethically according to the Guide for the Care and Use of Laboratory Animals and institutional guidelines.

Quantitative RT-PCR assay

Total RNA was extracted from mouse tissues using Trizol reagent (ThermoFisher). cDNA synthesis was carried out on 1 μg of total RNA, using a HiScriptIII RT SuperMix (Vazyme, R323, Nanjing,China) according to the manufacturer's instructions. The cDNA (dilution 1:4) was then analyzed by quantitative RT-PCR in a typical reaction of 20 μl containing 250 nmol/l of forward and reverse primers, 1 μl of cDNA and AceQ qPCR SYBR Green Master Mix (Vazyme, Q131, Nanjing, China). The reaction was initiated by preheating at 50°C for 2 min, followed by 95°C for 5 min and 40 amplification cycles of 10s denaturation at 95°C and 30s annealing and extension at 60°C. Gene expression was normalized to 18s rRNA within the log phase of the amplification curve. The primer sequences are listed in Table S1.

Minigene splicing assay and verification of protein expression in vitro

Minigene splicing assay was carried out as described previously(Windpassinger et al., 2017). C20orf26 (NM_015585.4) minigenes containing exon2, a 357 bp fragment of the 5' flanking intron, a 238 bp fragment of the 3' flanking intron and differential for c.143+5 G>A mutation were amplified by PCR with oligos carrying the recombinant sites XhoI and BamHI. The PCR fragment was then cloned into the pET01 vector (MoBiTec, Goettingen, Germany). All minigene plasmids pET01 were sequenced to verify the correct insertion of mutated and wild-type DNA fragments. The splicing assay was performed by transiently transfecting

HEK293T cells with each plasmid using Lipofectamine 2000 (ThermoFisher). At 48 hours post-transfection, cells were harvested and total RNA was extracted and reserve-transcribed. The resulting cDNAs were amplified by PCR with the forward primer corresponding to upstream exon A and the reverse primer complementary to downstream exon B. The primer sequences were as follows: Forward 5'- CCAGTTGAGGAGGAGAAC -3'and reserve 5'- CCAAGGTCTGAAGGTCAC -3'. PCR products were separated by 2% agarose gel electrophoresis and fragments were analyzed by Sanger sequencing.

Based on the design of minigene assay, we amplified the sequence (intron1'-exon2-intron2') between exon A and exon B of the C20orf26 minigene plasmids described above, adding exon 1 and exon 3-33 of C20orf26 before and after this sequence, and then inserted them into eukaryotic overexpression vector pCAG1.1-3xFlag (provided by Prof. Masahito Ikawa, Osaka University) with BamHI and HindIII restriction sites. Besides, the firefly luciferase gene was introduced to be uesd as an internal control. HEK293T cell transfection was carried out in much the same way as indicated above. At 48 hours post-transfection, cells were harvested, half of the cell pellet was used for RNA extraction, followed by reserve-transcribed, and half was used for protein extraction, following western blot analysis. The primer sequences used for RT-PCR were as follows: C20orf26: 5'-TGGAGTGCGGCGTCCTGGA-3', 5'- CCCGGAACACTGACACCCAGTC-3'; Firefly luciferase: 5'-TGAGGTGGACATCACCTATGC-3', 5'-CGCTCGTTGTAAATGTCGTTA-3'.

Antibodies

Rabbit antibodies specific for RSPH9 (23253-1-AP), NME5 (12923-1-AP), DNAJB13 (25118-1-AP), DYNLL2 (16811-1-AP), SLC2A3 (20403-1-AP), IFT74 (27334-1-AP), PPP1CC(11082-1-AP) and Firefly Luciferase(27986-1-AP) were purchased from Proteintech (Rosemont, IL, USA).A Rabbit antibody specific for β-Actin (ab8229) was purchased from Abcam. Mouse anti-FLAG M2 (F3165) used for western blot and mouse anti-Acetylated Tubulin (T6793) were purchased from Sigma-Aldrich. The rabbit antibody specific for the DDDDK-tag (PM020) used for co-immunoprecipitation and the mouse antibody specific for HA-tag (M180-3) were purchased from Medical & Biological Laboratories (Nagoya, JP). Mouse anti-AKAP4 (611564) was purchased from BD Biosciences (California, USA). Mouse anti- casein kinase IIα' (sc-514403) was purchased from Santa Cruz (CA, USA).

The specific antibody for CFAP61 was generated according to the published method (Liu et al., 2014). Briefly, mouse CFAP61 (aa 223–348 and aa 1103-1230) was expressed as His fusion proteins in E.coli using the pET-28a(+) vector, then the fusion proteins were affinity purified with Ni-NTA His Bind Resin. Two rabbits and two mice were immunized with the fusion protein, respectively. The resulting working antisera are anti-CFAP61.

Generation of *Cfap61*$^{-/-}$ Mice by CRISPR/Cas9

The *Cfap61* knockout mice were generated using CRISPR/Cas9 genome editing as described below. In brief, we selected two sgRNA targets to generate a deletion of the exon4 of *Cfap61* in mouse. The target sequences of sgRNA were 5'-GCTGTTTATGCACTTCTTTGTGG-3' and 5'-GATTTCTTTGAGGCAGCCAGTGG -3'. The two complementary DNA oligos of each sgRNA target were annealed and ligated to the BsaI-digested pUC57-T7-sgRNA vector. The sgRNA templates were obtained from sgRNA plasmids by PCR amplification with primers Trans PCR For (5'-GAAATTAATACGACTCACTATAGG-3') and Trans PCR Rev (5'-AAAAGCACCGACTCGGTGCCA-3'). Then, the PCR products were purified using a MinElute PCR Purification Kit (28004, QIAGEN). Two sgRNA were produced using the MEGAshortscript Kit (AM1354, Ambion) and purified using the MEGAclear Kit (AM1908, Ambion) according to the manufacturer's instructions. The Cas9 plasmid (Addgene No. 44758) was linearized with AgeI and then purified using a MinElute PCR Purification Kit (28004, QIAGEN). Cas9 mRNA was produced by *in vitro* transcription using a mMESSAGE mMACHINE T7 Ultra Kit (AM1345, Ambion) and purified using a RNeasy Mini Kit (74104, QIAGEN) per the manufacturer's instructions. Mouse zygotes were coinjected with Cas9 mRNA (50 ng/μL), sgRNA (20 ng/μL). The injected zygotes were transferred into pseudo-pregnant recipients. The newborn mice (7 days old) were tagged by a toe cut, and DNA was extracted using the Mouse Direct PCR Kit (B40013, Biotool). PCR amplification was carried out with primers (Forward: 5'- AGGCAGTGAGTGAAGTGT -3', Reverse: 5'-TAAGTTGGCGAGGCTTGA -3') using PrimeSTAR HS DNA Polymerase (DR010A, Takara) under the following conditions: 95^{o} C for 5 min; 35 cycles of 95^{o} C for 30 s, 62^{o} C ($^{-}$ 0.2^{o} C/cycle) for 30 s, and 72^{o} C for 30s; and a final step of 72^{o} C for 5 min. The PCR products were subjected to Sanger sequencing.

Fertility Test

Adult mice from each genotype were subjected to fertility tests in which each male was mated with three wild-type C57BL/6 female mice, and the vaginal plug was checked every morning. The dates of birth and number of pups in each litter were recorded.

Sperm Analysis

Epididymal sperm was obtained by making small incisions throughout the cauda of the epididymis, followed by extrusion and suspension in human tubal fluid culture medium (In Vitro Care, Frederick, MD, USA) supplemented with 10% FBS at 37 °C. Sperm samples (10 μl) were used for computer-assisted semen analysis (Hamilton-Thorne Research, Inc., Beverly,MA, USA). The remaining of sperm samples were fixed in 4% paraformaldehyde for 30min and subsequently spread on slides. The H&E staining was conducted using standard methods for sperm morphology study. Over 200 spermatozoa were examined, and morphological abnormalities were evaluated as described previously (Li et al., 2020) following the WHO guidelines. Each spermatozoon was classified in only one morphological category according to its major flagellar abnormality.

Histological Analysis

Mouse testes, epididymis and tracheas were collected from at least three mice for each genotype. The testes and epididymis were fixed in modified Davidson's fluid for up to 24 h while tracheas were fixed in 4% paraformaldehyde in PBS overnight and stored in 70% ethanol. The samples were then dehydrated through a graded ethanol series and embedded in paraffin. Tissue sections (thickness 5μm) were prepared and mounted on glass slides and HE staining was performed according to standard procedures. Periodic Acid-Schiff (PAS) staining was carried out using the Sigma Aldrich PAS staining kit (395B).

Transmission electron microscopy (TEM)

Ultrastructural examination were performed as described below. Briefly, the epididymal sperm was fixed with 2.5% glutaraldehyde overnight,postfixed with 2% OsO4 and embedded in Araldite. Ultrathin sections (80 nm) were stained with uranyl acetate and lead citrate and analyzed by an electron microscope (JEM.1010, JEOL).

Scanning electron microscopy (SEM)

Spermatozoa and trachea from normal and *Cfap61*-mutated male mice were fixed in 2.5% phosphate-buffered glutaraldehyde at 4°C for 2 hours. Immobilized spermatozoa were deposited on poly-L-lysine coated coverslips. Subsequently, spermatozoa and trachea were washed in PBS solution, dehydrated via an ascending gradient of cold 30%, 50%, 70%, 80%, 90% and 100% ethanol, and dried at critical point using a Leica EM CPD300 Critical Point Dryer (Wetzlar, Germany). Specimens were then attached to specimen holders and coated with gold particles using an ion sputter coater (EM ACE200, Leica, Wetzlar, Germany) before being viewed with a Helios G4 CX scanning electron microscope (Thermo scientific).

Fractionation of spermatozoa

Sperm protein fractionation was performed as described previously (Castaneda et al., 2017). Spermatozoa were suspended in 1% TritonX-100 lysis buffer (50 mM NaCl, 20 mM Tris·HCl, pH 7.5, protease inhibitor mixture) and incubated at 4 °C for 2 h. The sample was centrifuged at 15,000 × g for 10 min to separate the Triton-soluble fraction (supernatant) and the Triton-resistant fraction (pellet). The pellet was resuspended in 1% SDS lysis buffer (75 mM NaCl, 24 mM EDTA, pH 6.0) and incubated at room temperature for 1 h. The sample was centrifuged at 15,000 × g for 10 min to separate SDS-soluble fraction (supernatant) and SDS-resistant fraction (pellet). The pellet was dissolved in sample buffer and boiled for 10 min.

Western blot analysis

Western blotting was performed as described below. Briefly, protein extracts were prepared using lysis buffer (8 M urea, 50mM Tris-HCl pH 8.2, 75Mm NaCl) in the presence of 1x cOmpleteTM EDTA-free Protease Inhibitor Cocktail (Roche, Basel, Switzerland). The proteins were separated by SDS-PAGE and transferred onto a polyvinylidene difluoride membrane. The membrane was blocked with 5% non-fat milk in TBS solution for 2 h at room temperature and incubated overnight at 4ºC with primary antibodies diluted in 5% bovine serum albumin (BSA) at 1:2000. The membranes were washed with TBST (0.1% Tween-20 in TBS) buffer three times and incubated at room temperature for 2 h with secondary antibodies diluted in 5% no-fat milk at 1:5000. The signals from the detected proteins were visualized using SuperSignal West Femto Chemiluminescent Substrate (Thermofisher).

Plasmids construction

Full-length cDNA encoding Cfap61, Rsph3a, Rsph9, Ropn1, Ropn1l, Caml4, Armc4, Dynll2, Maats1, Dynltla, Dyncli2, Dynll1, Dynlrb2, Ift22, Ift74, Ift81 and Wdr35 were amplified by PCR with oligos carrying the recombinant sites and cloned into pcDNA3.1(+) vector (Thermofisher) in which a FLAG or HA epiptope was introduced prior to the multicloning site. The primers used to amplify each gene are listed in Table S2. *Chlamydomonas* genes were chemically synthesized by GenScript (Nanjing,China) and inserted individually into vector plasmid pcDNA3.1(+)-N-HA or pcDNA3.1(+)-N-FLAG.

Cell culture

HEK293T cells were were purchased from ATCC and maintained in DMEM high glucose supplemented with 10% fetal bovine serum (Gibco), Penicillin-Streptomycin (100U/ml,Thermofisher). Transfections of HEK293T cells were performed using using Lipofectamine 2000 (11668019, ThermoFisher) according to manufacturer's instructions.

Proximity ligation assay (PLA)

Duolink in situ proximity ligation assays were carried according to the manufacturer's instructions (DUO920102, Sigma-aldrich). Briefly, isolated sperm cells were smeared onto slides, air-dried, fixed for 40 min with 4% paraformaldehyde, washed thrice with PBS (5 min/wash), followed by blocking with Duolink blocking solution for 60 minutes at 37˚C. Primary antibodies were diluted in Duolink antibody diluent and incubated overnight at 4˚C. Appropriate secondary antibodies conjugated to synthetic oligonucleotides (anti-rabbit PLUS and anti-mouse MINUS) were applied for one hour at 37˚C. A ligation reaction was performed using the Duolink ligation solution and ligase at 37˚C for 30 minutes, which results in binding of the two PLA probes if they are less than 40 nanometres from one another. Rolling circle amplification and hybridisation with fluorescently labelled nucleotides was achieved using the Duolink amplification solution and polymerase at 37˚C for 100 minutes. Slides were mounted with Duolink mounting medium with DAPI, and imaged with a TCS SP8X confocal microscope (Leica Microsystems, Wetzlar, Germany).

Immunoprecipitation

Two days after transfection, cells were lysed with RIPA Lysis Buffer (P0013C, Beyotime) supplemented with 1x cOmplete^{TM} EDTA-free Protease Inhibitor Cocktail (Roche, Basel, Switzerland) for 40 min at 4°C and then clarified by centrifugation at 12,000 × g for 20 min.

The lysates were precleared with 10 µL ProteinA magnetic beads (10008D, ThermoFisher) for 1 h at 4°C. Precleared lysates were incubated overnight with Anti-DDDDK-tag at 4°C. Lysates were then incubated with 50 µL Protein A magnetic beads for 4h at 4°C. The beads were washed three times with RIPA Lysis Buffer and boiled for 5min in SDS loading buffer before SDS/PAGE.

CFAP61 was immunoprecipitated from mouse testis using the Pierce crosslink IP kit (26147, Thermo Scientific) with anti-CFAP61 antibody described above, IP was performed according to the manufacturer's instructions. Half of IP eluates were boiled in SDS loading buffer and analyzed by standard WB procedures, the other half were futher analyzed by mass spectrometry.

Mass spectrometry

Eluates were precipitated with five volumes of -20℃ pre-chilled acetone followed by trypsin digestion. LC-MS/MS analysis was performed on EASY-nanoLC 1000 system (Thermo Scientific) coupled to an Orbitrap Fusion Tribrid mass spectrometer (Thermo Scientific) by a nano spray ion source. Tryptic peptide mixtures were injected automatically and loaded at a flow rate of 20 µl/min in 0.1% formic acid in LC-grade water onto an analytical column (Acclaim PepMap C18, 75 µm x 25 cm; Thermo Scientific). The peptide mixture was separated by a linear gradient from 5% to 38% of buffer B (0.1% formic acid in ACN) at a flow rate of 300 nl/min over 53 minutes. Remaining peptides were eluted by a short gradient from 38% to 90% buffer B in 1 minutes. Analysis of the eluted peptides was done on an Orbitrap Fusion Tribrid mass spectrometer. From the high-resolution MS pre-scan with a mass range of 335 to 1400, the most intense peptide ions were selected for fragment analysis in the orbitrap depending by using a high speed method if they were at least doubly charged. The normalized collision energy for HCD was set to a value of 28 and the resulting fragments were detected with a resolution of 120,000. The lock mass option was activated; the background signal with a mass of 445.12003 was used as lock mass. Every ion selected for fragmentation was excluded for 30 seconds by dynamic exclusion. Data were processed with MaxQuant software (version 1.6.10.43) and Mouse reference proteome from SwissProt database (release 2019_07) using standard parameters.The partial mass spectrometry proteomics data have been deposited to the ProteomeXchange Consortium via the PRIDE partner repository with the dataset identifer PXD024469.

Immunofluorescence

For testis and trachea cryosections, immunostaining was performed as previously described(Castañeda et al., 2014). For spermatozoa, samples were obtained as described above. For germ cells, samples were squeezed out from the seminiferous tubules onto slide glasses and air-dried at room temperature. The samples were then fixed with 4% paraformaldehyde in PBS for 30 min. After three 10-min washes with PBS, heat-induced antigen retrieval was carried out by boiling the slides in 10 mM citrate buffer (pH 6.0) in a microwave oven for 10 min. After three 10-min washes with PBST (0.1% Triton X-100 in PBS), the slides were blocked with 5% bovine serum albumin (BSA) diluted in PBST for 1 h and then incubated with primary antibodies (1:200) at 4ºC overnight. After incubation with the secondary antibody (1:500) at room temperature for 2 h, the slides were incubated with Hoechst 33342 for 5 min. Finally, the slides were washed in PBS and then mounted with VectaShield or Immu-Mount. Slides were viewed with an LSM800 confocal microscope (Carl Zeiss AG) or TCS SP8X confocal microscope (Leica Microsystems, Wetzlar, Germany).

Recording of cilia motility in trachea

Mouse trachea were removed by dissection and placed in DMEM high glucose supplemented with 10% fetal bovine serum (Gibco). Trachea were opened on the dorsal side and cut into 5 mm squares under a stereoscopic microscope. The tissue pieces were observed in a confocal dish (BDD012035, BIOFIL) on a glass slide (801011, NEST) with a scotch tape spacer under a 40× objective (CFI S Plan Flour ELWD NAMC) of an inverted microscope (Eclipse Ti2-U, Nikon).

Statistical analysis.

All experiments were repeated at least three times. The differences between treatment and control groups were analyzed using one-way ANOVA or unpaired two-tailed t-tests. P-values < 0.05 were considered statistical significance. All data represent the mean ± the standard error of the mean. Analyses were performed using the Microsoft Excel or GraphPad Prism 6.0.

Acknowledgements

We would like to thank Prof. Bin Shen (Nanjing Medical University) for providing us with pET01 plasmid. Vector pCAG1.1-3xFlag was a kind gift from Prof. Masahito Ikawa (Osaka University). We are grateful to Jiaxiong Wang, the examiner of Suzhou Hospital Affiliated to Nanjing Medical University for his help in morphological classification of abnormal sperm flagella.

Competing interests

The authors declare no competing interests.

Funding

This work was supported by the National Key Research and Development Program of China 2016YFA0500902 (to M.L.); Natural Science Foundation of China (32070842, 31771654 and 31530047 to M.L.); the Natural Science Foundation of Jiangsu Province (Grants No. BK20190081 to M.L.); and Qing Lan Project (to M.L.); the FLAGEL-OME project (to P. F. Ray) : ANR-19-CE17-001.

Data availability

The mass spectrometry proteomics data have been deposited to the ProteomeXchange Consortium via the PRIDE partner repository with the dataset identifier PXD024469.

References

ABBASI, F., MIYATA, H., SHIMADA, K., MOROHOSHI, A., NOZAWA, K., MATSUMURA, T., XU, Z., PRATIWI, P. & IKAWA, M. 2018. RSPH6A is required for sperm flagellum formation and male fertility in mice. *J Cell Sci,* 131.

AFZELIUS, B. A. & ELIASSON, R. 1983. Male and female infertility problems in the immotile-cilia syndrome. *Eur J Respir Dis Suppl,* 127**,** 144-7.

ARAFAH, K., LOPEZ, F., CAZIN, C., KHERRAF, Z.-E., TASSISTRO, V., LOUNDOU, A., ARNOULT, C., THIERRY-MIEG, N., BULET, P., GUICHAOUA, M.-R., et al. 2020. Defect in the nuclear pore membrane glycoprotein 210-like gene is associated with extreme uncondensed sperm nuclear chromatin and male infertility: a case report. *Human Reproduction*.

AUGUSTE, Y., DELAGUE, V., DESVIGNES, J.-P., LONGEPIED, G., GNISCI, A., BESNIER, P., LEVY, N., BEROUD, C., MEGARBANE, A., METZLER-GUILLEMAIN, C., et al. 2018. Loss of Calmodulin- and Radial-Spoke-Associated Complex Protein CFAP251 Leads to Immotile Spermatozoa Lacking Mitochondria and Infertility in Men. *The American Journal of Human Genetics,* 103**,** 413-420.

BEN KHELIFA, M., COUTTON, C., ZOUARI, R., KARAOUZENE, T., RENDU, J., BIDART, M., YASSINE, S., PIERRE, V., DELAROCHE, J., HENNEBICQ, S., et al. 2014. Mutations in DNAH1, which encodes an inner arm heavy chain dynein, lead to male infertility from multiple morphological abnormalities of the sperm flagella. *Am J Hum Genet,* 94**,** 95-104.

BEUROIS, J., MARTINEZ, G., CAZIN, C., KHERRAF, Z. E., AMIRI-YEKTA, A., THIERRY-MIEG, N., BIDART, M., PETRE, G., SATRE, V., BROUILLET, S., et al. 2019. CFAP70 mutations lead to male infertility due to severe astheno-teratozoospermia. A case report. *Hum Reprod,* 34**,** 2071-2079.

CASTAñEDA, J., GENZOR, P., VAN DER HEIJDEN, G. W., SARKESHIK, A., YATES, J. R., 3RD, INGOLIA, N. T. & BORTVIN, A. 2014. Reduced pachytene piRNAs and translation underlie spermiogenic arrest in Maelstrom mutant mice. *Embo j,* 33**,** 1999-2019.

CASTANEDA, J. M., HUA, R., MIYATA, H., OJI, A., GUO, Y., CHENG, Y., ZHOU, T., GUO, X., CUI, Y., SHEN, B., et al. 2017. TCTE1 is a conserved component of the dynein regulatory complex and is required for motility and metabolism in mouse spermatozoa. *Proc Natl Acad Sci U S A,* 114**,** E5370-e5378.

COUTTON, C., ESCOFFIER, J., MARTINEZ, G., ARNOULT, C. & RAY, P. F. 2015. Teratozoospermia: spotlight on the main genetic actors in the human. *Hum Reprod Update,* 21**,** 455-85.

COUTTON, C., MARTINEZ, G., KHERRAF, Z. E., AMIRI-YEKTA, A., BOGUENET, M., SAUT, A., HE, X., ZHANG, F., CRISTOU-KENT, M., ESCOFFIER, J., et al. 2019. Bi-allelic Mutations in ARMC2 Lead to Severe Astheno-Teratozoospermia Due to Sperm Flagellum Malformations in Humans and Mice. *Am J Hum Genet,* 104**,** 331-340.

COUTTON, C., VARGAS, A. S., AMIRI-YEKTA, A., KHERRAF, Z. E., BEN MUSTAPHA, S. F., LE TANNO, P., WAMBERGUE-LEGRAND, C., KARAOUZèNE, T., MARTINEZ, G., CROUZY, S., et al. 2018. Mutations in CFAP43 and CFAP44 cause male infertility and flagellum defects in Trypanosoma and human. *Nat Commun,* 9**,** 686.

CURRY, A. M., WILLIAMS, B. D. & ROSENBAUM, J. L. 1992. Sequence analysis reveals homology between two proteins of the flagellar radial spoke. *Mol Cell Biol,* 12**,** 3967-77.

DIENER, D. R., YANG, P., GEIMER, S., COLE, D. G., SALE, W. S. & ROSENBAUM, J. L. 2011. Sequential assembly of flagellar radial spokes. *Cytoskeleton,* 68**,** 389-400.

DONG, F. N., AMIRI-YEKTA, A., MARTINEZ, G., SAUT, A., TEK, J., STOUVENEL, L., LORèS, P., KARAOUZèNE, T., THIERRY-MIEG, N., SATRE, V., et al. 2018. Absence of CFAP69 Causes Male Infertility due to Multiple Morphological Abnormalities of the Flagella in Human and Mouse. *Am J Hum Genet,* 102**,** 636-648.

DUTCHER, S. K., MOROHOSHI, A., MIYATA, H., SHIMADA, K., NOZAWA, K., MATSUMURA, T., YANASE, R., SHIBA, K., INABA, K. & IKAWA, M. 2020. Nexin-Dynein regulatory complex component DRC7 but not FBXL13 is required for sperm flagellum formation and male fertility in mice. *PLOS Genetics,* 16.

DYMEK, E. E. & SMITH, E. F. 2007. A conserved CaM- and radial spoke–associated complex mediates regulation of flagellar dynein activity. *Journal of Cell Biology,* 179**,** 515-526.

FLIEGAUF, M., BENZING, T. & OMRAN, H. 2007. When cilia go bad: cilia defects and ciliopathies. *Nat Rev Mol Cell Biol,* 8**,** 880-93.

HE, X., LI, W., WU, H., LV, M., LIU, W., LIU, C., ZHU, F., LI, C., FANG, Y., YANG, C., et al. 2019. Novel homozygous CFAP69 mutations in humans and mice cause severe asthenoteratospermia with multiple morphological abnormalities of the sperm flagella. *Journal of Medical Genetics,* 56**,** 96-103.

HE, X., LIU, C., YANG, X., LV, M., NI, X., LI, Q., CHENG, H., LIU, W., TIAN, S., WU, H., et al. 2020. Bi-allelic Loss-of-function Variants in CFAP58 Cause Flagellar Axoneme and Mitochondrial Sheath Defects and Asthenoteratozoospermia in Humans and Mice. *The American Journal of Human Genetics,* 107**,** 514-526.

HEUSER, T., DYMEK, E. E., LIN, J., SMITH, E. F. & NICASTRO, D. 2012. The CSC connects three major axonemal complexes involved in dynein regulation. *Mol Biol Cell,* 23**,** 3143-55.

HUANG, T., YIN, Y., LIU, C., LI, M., YU, X., WANG, X., ZHANG, H., MUHAMMAD, T., GAO, F., LI, W., et al. 2020. Absence of murine CFAP61 causes male infertility due to multiple morphological abnormalities of the flagella. *Science Bulletin,* 65**,** 854-864.

IBANEZ-TALLON, I., HEINTZ, N. & OMRAN, H. 2003. To beat or not to beat: roles of cilia in development and disease. *Hum Mol Genet,* 12 Spec No 1**,** R27-35.

KHERRAF, Z. E., AMIRI-YEKTA, A., DACHEUX, D., KARAOUZèNE, T., COUTTON, C., CHRISTOU-KENT, M., MARTINEZ, G., LANDREIN, N., LE TANNO, P., FOURATI BEN MUSTAPHA, S., et al. 2018. A Homozygous Ancestral SVA-Insertion-Mediated Deletion in WDR66 Induces Multiple Morphological Abnormalities of the Sperm Flagellum and Male Infertility. *Am J Hum Genet,* 103**,** 400-412.

KING, S. M. & PATEL-KING, R. S. 1995. The M(r) = 8,000 and 11,000 outer arm dynein light chains from Chlamydomonas flagella have cytoplasmic homologues. *J Biol Chem,* 270**,** 11445-52.

LECHTRECK, K. F. 2015. IFT–Cargo Interactions and Protein Transport in Cilia. *Trends in Biochemical Sciences,* 40**,** 765-778.

LI, W., HE, X., YANG, S., LIU, C., WU, H., LIU, W., LV, M., TANG, D., TAN, J., TANG, S., et al. 2019. Biallelic mutations of CFAP251 cause sperm flagellar defects and human male infertility. *J Hum Genet,* 64**,** 49-54.

LI, W., WU, H., LI, F., TIAN, S., KHERRAF, Z. E., ZHANG, J., NI, X., LV, M., LIU, C., TAN, Q., et al. 2020. Biallelic mutations in CFAP65 cause male infertility with multiple morphological abnormalities of the sperm flagella in humans and mice. *J Med Genet,* 57**,** 89-95.

LINDEMANN, C. B. & LESICH, K. A. 2016. Functional anatomy of the mammalian sperm flagellum. *Cytoskeleton (Hoboken),* 73**,** 652-669.

LIU, C., HE, X., LIU, W., YANG, S., WANG, L., LI, W., WU, H., TANG, S., NI, X., WANG, J., et al. 2019a. Bi-allelic Mutations in TTC29 Cause Male Subfertility with Asthenoteratospermia in Humans and Mice. *The American Journal of Human Genetics,* 105**,** 1168-1181.

LIU, C., MIYATA, H., GAO, Y., SHA, Y., TANG, S., XU, Z., WHITFIELD, M., PATRAT, C., WU, H., DULIOUST, E., et al. 2020. Bi-allelic DNAH8 Variants Lead to Multiple Morphological Abnormalities of the Sperm Flagella and Primary Male Infertility. *Am J Hum Genet,* 107**,** 330-341.

LIU, M., SHI, X., BI, Y., QI, L., GUO, X., WANG, L., ZHOU, Z. & SHA, J. 2014. SHCBP1L, a conserved protein in mammals, is predominantly expressed in male germ cells and maintains spindle stability during meiosis in testis. *Mol Hum Reprod,* 20**,** 463-75.

LIU, W., HE, X., YANG, S., ZOUARI, R., WANG, J., WU, H., KHERRAF, Z. E., LIU, C., COUTTON, C., ZHAO, R., et al. 2019b. Bi-allelic Mutations in TTC21A Induce Asthenoteratospermia in Humans and Mice. *Am J Hum Genet,* 104**,** 738-748.

LIU, W., SHA, Y., LI, Y., MEI, L., LIN, S., HUANG, X., LU, J., DING, L., KONG, S. & LU, Z. 2019c. Loss-of-function mutations in SPEF2 cause multiple morphological abnormalities of the sperm flagella (MMAF). *Journal of Medical Genetics,* 56**,** 678-684.

LORèS, P., COUTTON, C., EL KHOURI, E., STOUVENEL, L., GIVELET, M., THOMAS, L., RODE, B., SCHMITT, A., LOUIS, B., SAKHELI, Z., et al. 2018. Homozygous missense mutation L673P in adenylate kinase 7 (AK7) leads to primary male infertility and multiple morphological anomalies of the flagella but not to primary ciliary dyskinesia. *Hum Mol Genet,* 27**,** 1196-1211.

LUCAS, J. S., BURGESS, A., MITCHISON, H. M., MOYA, E., WILLIAMSON, M., HOGG, C. & NATIONAL PCD SERVICE, U. K. 2014. Diagnosis and management of primary ciliary dyskinesia. *Arch Dis Child,* 99**,** 850-6.

LV, M., LIU, W., CHI, W., NI, X., WANG, J., CHENG, H., LI, W.-Y., YANG, S., WU, H., ZHANG, J., et al. 2020. Homozygous mutations in DZIP1 can induce asthenoteratospermia with severe MMAF. *Journal of Medical Genetics,* 57**,** 445-453.

LYONS, R. A., SARIDOGAN, E. & DJAHANBAKHCH, O. 2006. The reproductive significance of human Fallopian tube cilia. *Hum Reprod Update,* 12**,** 363-72.

MARTINEZ, G., BEUROIS, J., DACHEUX, D., CAZIN, C., BIDART, M., KHERRAF, Z. E., ROBINSON, D. R., SATRE, V., LE GAC, G., KA, C., et al. 2020. Biallelic variants in MAATS1 encoding CFAP91, a calmodulin-associated and spoke-associated complex protein, cause severe astheno-teratozoospermia and male infertility. *J Med Genet,* 57**,** 708-716.

MARTINEZ, G., KHERRAF, Z. E., ZOUARI, R., FOURATI BEN MUSTAPHA, S., SAUT, A., PERNET-GALLAY, K., BERTRAND, A., BIDART, M., HOGRAINDLEUR, J. P., AMIRI-YEKTA, A., et al. 2018. Whole-exome sequencing identifies mutations in FSIP2 as a recurrent cause of multiple morphological abnormalities of the sperm flagella. *Hum Reprod,* 33**,** 1973-1984.

MORYAN, A., GUAY, A. T., KURTZ, S. & NOWAK, P. J. 1985. Familial ciliary dyskinesis: a cause of infertility without respiratory disease. *Fertil Steril,* 44**,** 539-42.

MUNRO, N. C., CURRIE, D. C., LINDSAY, K. S., RYDER, T. A., RUTMAN, A., DEWAR, A., GREENSTONE, M. A., HENDRY, W. F. & COLE, P. J. 1994. Fertility in men with primary ciliary dyskinesia presenting with respiratory infection. *Thorax,* 49**,** 684-7.

ONOUFRIADIS, A., PAFF, T., ANTONY, D., SHOEMARK, A., MICHA, D., KUYT, B., SCHMIDTS, M., PETRIDI, S., DANKERT-ROELSE, J. E., HAARMAN, E. G., et al. 2013. Splice-site mutations in the axonemal outer dynein arm docking complex gene CCDC114 cause primary ciliary dyskinesia. *Am J Hum Genet,* 92**,** 88-98.

PATEL-KING, R. S., GORBATYUK, O., TAKEBE, S. & KING, S. M. 2004. Flagellar radial spokes contain a Ca2+-stimulated nucleoside diphosphate kinase. *Mol Biol Cell,* 15**,** 3891-902.

PIGINO, G., BUI, K. H., MAHESHWARI, A., LUPETTI, P., DIENER, D. & ISHIKAWA, T. 2011. Cryoelectron tomography of radial spokes in cilia and flagella. *Journal of Cell Biology,* 195**,** 673-687.

PIPERNO, G., HUANG, B., RAMANIS, Z. & LUCK, D. J. 1981. Radial spokes of Chlamydomonas flagella: polypeptide composition and phosphorylation of stalk components. *J Cell Biol,* 88**,** 73-9.

QIN, H., DIENER, D. R., GEIMER, S., COLE, D. G. & ROSENBAUM, J. L. 2004. Intraflagellar transport (IFT) cargo: IFT transports flagellar precursors to the tip and turnover products to the cell body. *J Cell Biol,* 164**,** 255-66.

RUBBO, B. & LUCAS, J. S. 2017. Clinical care for primary ciliary dyskinesia: current challenges and future directions. *Eur Respir Rev,* 26.

SATIR, P. 1968. Studies on cilia. 3. Further studies on the cilium tip and a "sliding filament" model of ciliary motility. *J Cell Biol,* 39**,** 77-94.

SHA, Y. W., XU, X., MEI, L. B., LI, P., SU, Z. Y., HE, X. Q. & LI, L. 2017. A homozygous CEP135 mutation is associated with multiple morphological abnormalities of the sperm flagella (MMAF). *Gene,* 633**,** 48-53.

SHEN, Y., ZHANG, F., LI, F., JIANG, X., YANG, Y., LI, X., LI, W., WANG, X., CHENG, J., LIU, M., et al. 2019. Loss-of-function mutations in QRICH2 cause male infertility with multiple morphological abnormalities of the sperm flagella. *Nature Communications,* 10.

SHINOHARA, K., CHEN, D., NISHIDA, T., MISAKI, K., YONEMURA, S. & HAMADA, H. 2015. Absence of Radial Spokes in Mouse Node Cilia Is Required for Rotational Movement but Confers Ultrastructural Instability as a Trade-Off. *Dev Cell,* 35**,** 236-46.

SINHA, N., PURI, P., NAIRN, A. C. & VIJAYARAGHAVAN, S. 2013. Selective ablation of Ppp1cc gene in testicular germ cells causes oligo-teratozoospermia and infertility in mice. *Biol Reprod,* 89**,** 128.

SöDERBERG, O., GULLBERG, M., JARVIUS, M., RIDDERSTRåLE, K., LEUCHOWIUS, K. J., JARVIUS, J., WESTER, K., HYDBRING, P., BAHRAM, F., LARSSON, L. G., et al. 2006. Direct observation of individual endogenous protein complexes in situ by proximity ligation. *Nat Methods,* 3**,** 995-1000.

TANG, S., WANG, X., LI, W., YANG, X., LI, Z., LIU, W., LI, C., ZHU, Z., WANG, L., WANG, J., et al. 2017. Biallelic Mutations in CFAP43 and CFAP44 Cause Male Infertility with Multiple Morphological Abnormalities of the Sperm Flagella. *The American Journal of Human Genetics,* 100**,** 854-864.

URBANSKA, P., SONG, K., JOACHIMIAK, E., KRZEMIEN-OJAK, L., KOPROWSKI, P., HENNESSEY, T., JERKA-DZIADOSZ, M., FABCZAK, H., GAERTIG, J., NICASTRO, D., et al. 2015. The CSC proteins FAP61 and FAP251 build the basal substructures of radial spoke 3 in cilia. *Molecular Biology of the Cell,* 26**,** 1463-1475.

VISWANADHA, R., SALE, W. S. & PORTER, M. E. 2017. Ciliary Motility: Regulation of Axonemal Dynein Motors. *Cold Spring Harbor Perspectives in Biology,* 9.

WHITFIELD, M., THOMAS, L., BEQUIGNON, E., SCHMITT, A., STOUVENEL, L., MONTANTIN, G., TISSIER, S., DUQUESNOY, P., COPIN, B., CHANTOT, S., et al. 2019. Mutations in DNAH17, Encoding a Sperm-Specific Axonemal Outer Dynein Arm Heavy Chain, Cause Isolated Male Infertility Due to Asthenozoospermia. *Am J Hum Genet,* 105**,** 198-212.

WILLIAMS, B. D., VELLECA, M. A., CURRY, A. M. & ROSENBAUM, J. L. 1989. Molecular cloning and sequence analysis of the Chlamydomonas gene coding for radial spoke protein 3: flagellar mutation pf-14 is an ochre allele. *J Cell Biol,* 109**,** 235-45.

WINDPASSINGER, C., PIARD, J., BONNARD, C., ALFADHEL, M., LIM, S., BISTEAU, X., BLOUIN, S., ALI, N. B., NG, A. Y. J., LU, H., et al. 2017. CDK10 Mutations in Humans and Mice Cause Severe Growth Retardation, Spine Malformations, and Developmental Delays. *Am J Hum Genet,* 101**,** 391-403.

XU, X., TOSELLI, P. A., RUSSELL, L. D. & SELDIN, D. C. 1999. Globozoospermia in mice lacking the casein kinase II alpha' catalytic subunit. *Nat Genet,* 23**,** 118-21.

YANG, C., COMPTON, M. M. & YANG, P. 2005. Dimeric novel HSP40 is incorporated into the radial spoke complex during the assembly process in flagella. *Mol Biol Cell,* 16**,** 637-48.

YANG, P., DIENER, D. R., YANG, C., KOHNO, T., PAZOUR, G. J., DIENES, J. M., AGRIN, N. S., KING, S. M., SALE, W. S., KAMIYA, R., et al. 2006. Radial spoke proteins of Chlamydomonas flagella. *J Cell Sci,* 119**,** 1165-74.

YANG, P., YANG, C. & SALE, W. S. 2004. Flagellar radial spoke protein 2 is a calmodulin binding protein required for motility in Chlamydomonas reinhardtii. *Eukaryot Cell,* 3**,** 72-81.

ZHANG, J., HE, X., WU, H., ZHANG, X., YANG, S., LIU, C., LIU, S., HUA, R., ZHOU, S., ZHAO, S., et al. 2021. Loss of DRC1 function leads to multiple morphological abnormalities of the sperm flagella and male infertility in human and mouse. *Hum Mol Genet*.

ZIMMER, W. E., SCHLOSS, J. A., SILFLOW, C. D., YOUNGBLOM, J. & WATTERSON, D. M. 1988. Structural organization, DNA sequence, and expression of the calmodulin gene. *J Biol Chem,* 263**,** 19370-83.

Figures

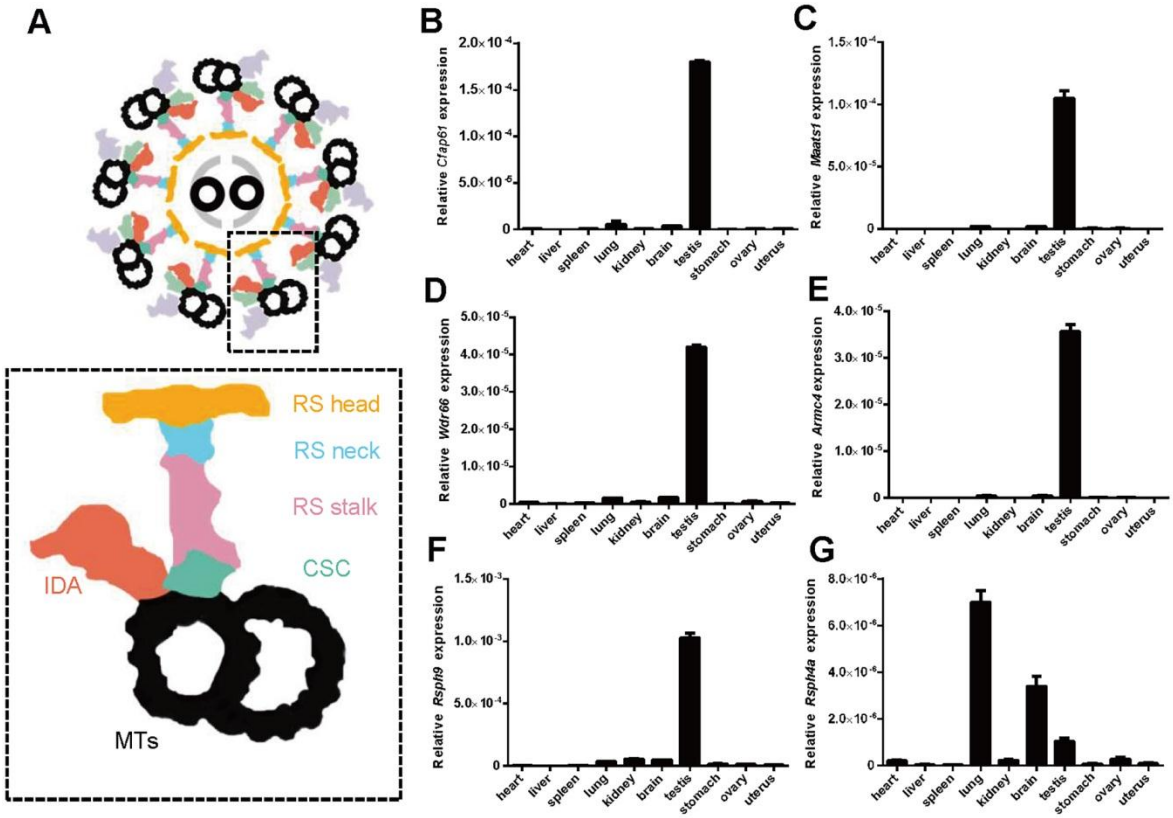

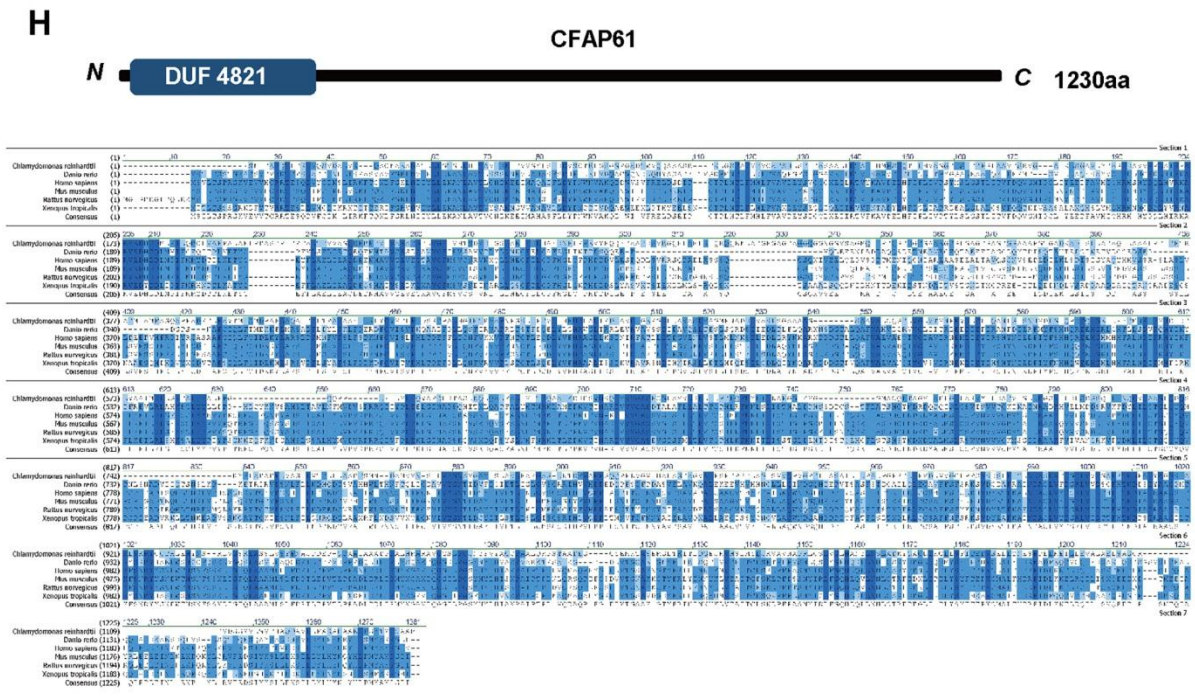

Fig. 1: *Cfap61* is an evolutionarily conserved testis-enriched gene.
(A) Schematic drawing of the flagella axoneme cross-section. Microtubules (MTs), inner dynein arm (IDA), radial spoke (RS) components and Calmodulin (CaM) and spoke associated complex (CSC) are indicated in the dotted box. (B-G) Quantitative RT–PCR results showing relative expression levels of *Rsph* and CSC genes in several mouse organs. (H) Sequence similarity of CFAP61 protein in various organisms. Dark blue background indicates identical residues in all species while blue background represents conserved residues. Light blue background shows weakly similar residues.

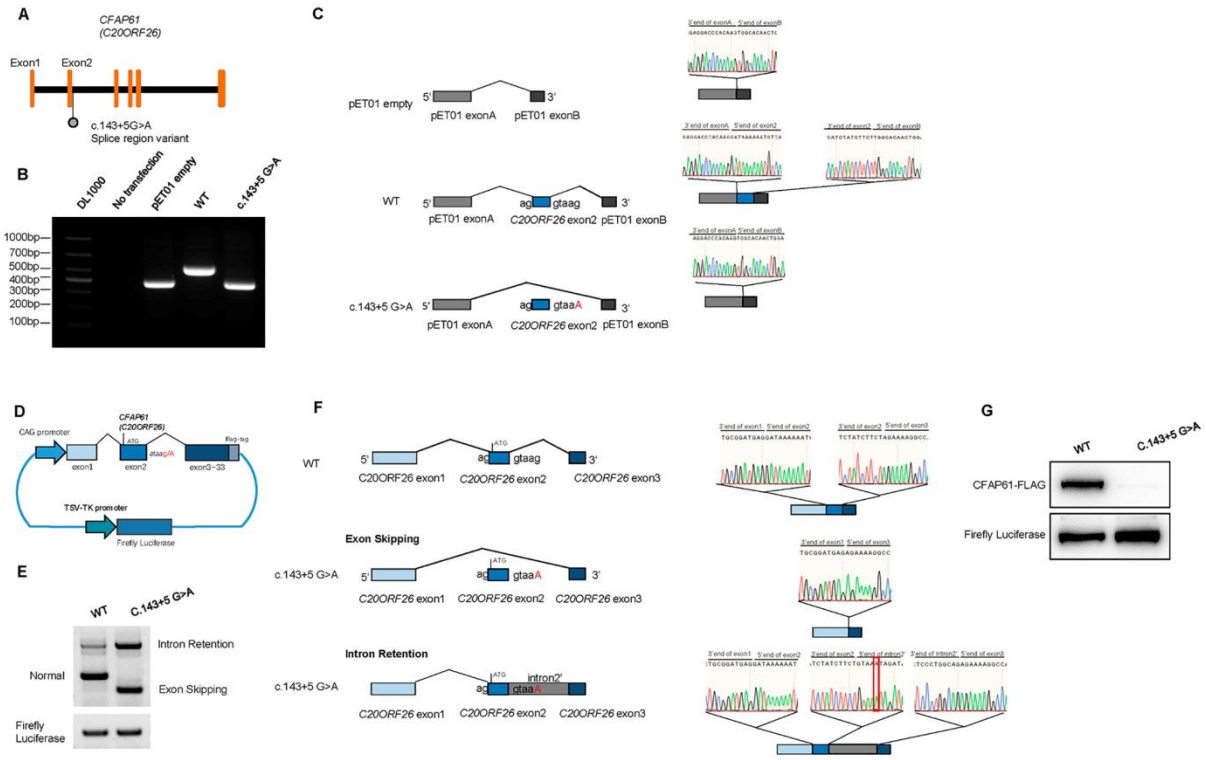

Fig. 2: Results of the minigene assay and splicing impact of the c.143+5 G>A mutation on *CFAP61*.

(A) A homozygous splice region variant: ENST00000245957.10:c.143+5G>A. Electrophoregrams of Sanger sequencing for PaCFAP61 and Control. (B) Gel electrophoresis of RT-PCR fragments from HEK293T cells transfected with plasmids carrying minigenes showed that c.143+5 G>A causes abnormal mRNA splicing. (C) Sanger sequencing confirmed that the c.143+5 G>A variant causes complete exon2 skipping. (D) Diagrams of the pCAG1.1-*CFAP61*-3xFlag construct . (E) Electrophoresis and sequencing of RT-PCR products from HEK293T cells transfected with pCAG1.1-*CFAP61*-3xFlag plasmids. (F) Sanger sequencing confirmed that the c.143+5 G>A variant causes both of exon skipping and intron retention. (G) Western blot analysis of CFAPF1 expression in HEK293T cells transfected with pCAG1.1-*CFAP61*-3xFlag plasmids, firefly luciferase served as a loading control.

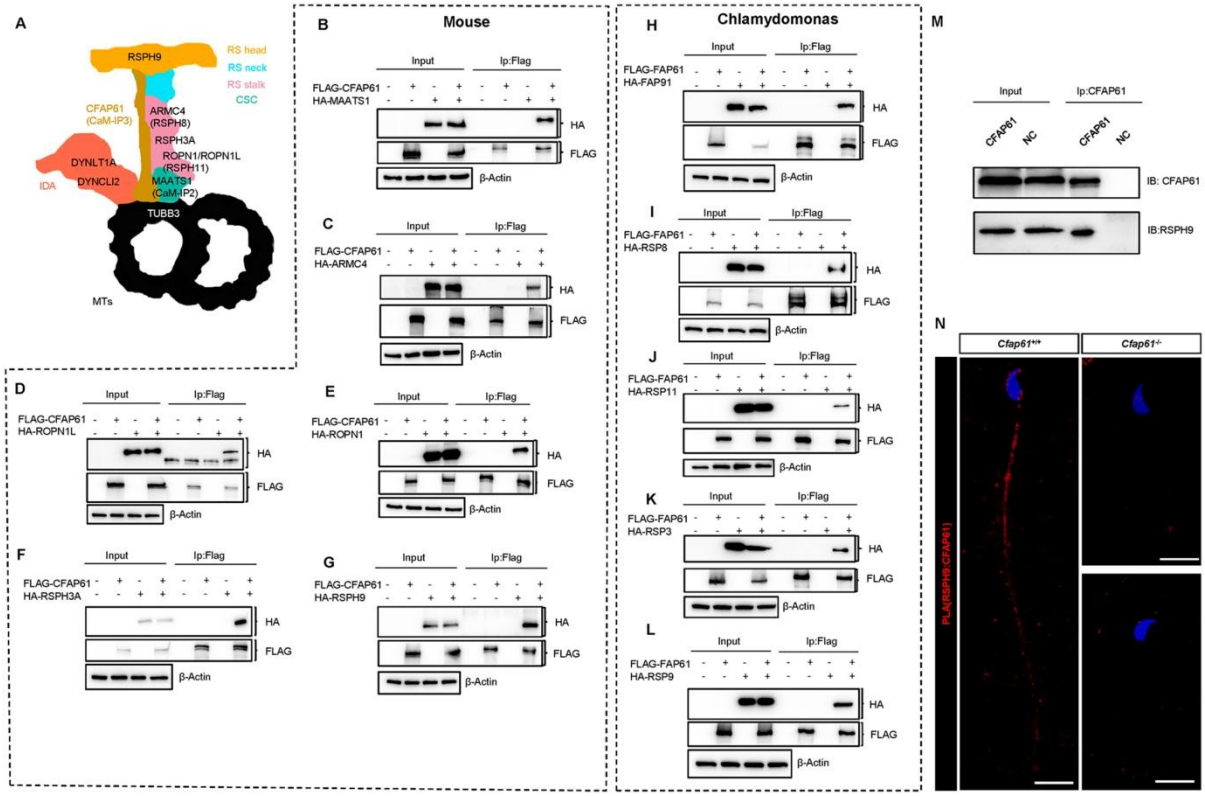

Fig. 3：CFAP61 is a component of radial spoke and CSC.

(A) Diagram of CFAP61 localization within the radial spoke and CSC. (B-L) Mouse and *Chlamydomonas* RS or CSC components were expressed or co-expressed with CFAP61 in HEK293T cells and CFAP61 interaction with other RS and CSC proteins was examined by co-immunoprecipitation with mouse (B-G) or *Chlamydomonas* (H-L) proteins. (M) Co-IP analysis of CFAP61 and RSPH9 from testicular protein extracts. (N) Representative immunofluorescence image from proximity ligation assay (PLA) performed on epididymal sperm from wild-type and *Cfap61*$^{-/-}$mice. Evidence of proximity (distance < 40 nm) between CFAP61 and RSPH9 is indicated by the appearance of red dots. Sperm heads were stained with DAPI (blue).

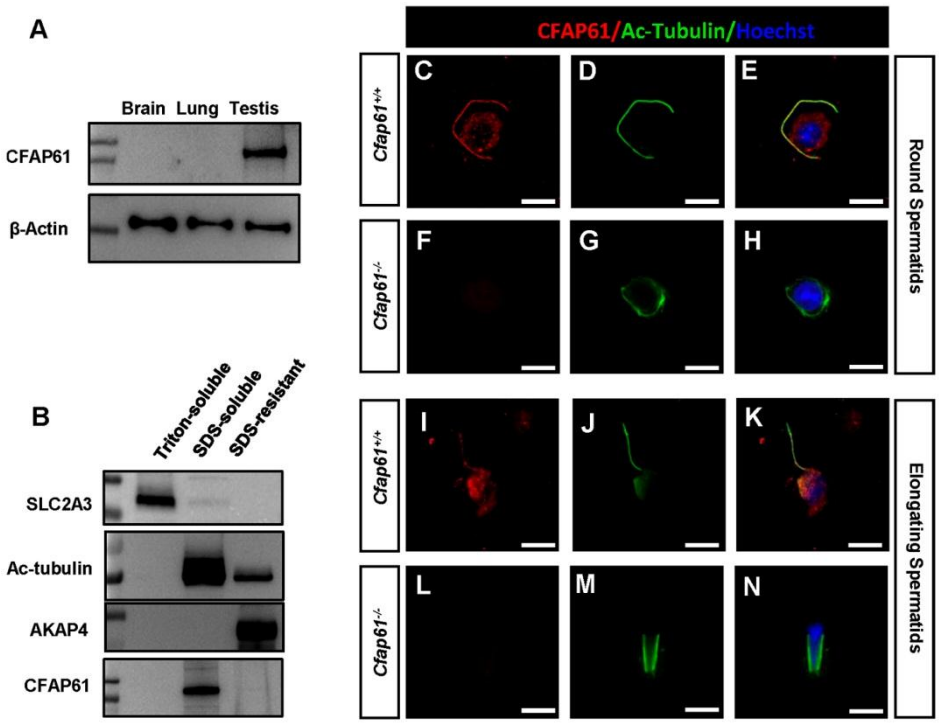

Fig. 4：CFAP61 localizes to sperm tails.

(A) Western blot analysis of protein extracts from brain, lung, and testis. (B) Western blot analysis of sperm fractionated into Triton X-100 soluble, SDS soluble, and SDS insoluble fractions from wild-type mice. SLC2A3, acetylated tubulin and AKAP4 were detected as markers for Triton-soluble, SDS-soluble and SDS-resistant fractions, respectively. (C-N) Immunofluorescence analysis of round and elongating spermatids from wild-type and *Cfap61*$^{-/-}$ mice using anti-CFAP61 (red) and anti-acetylated tubulin (green) antibodies. Scale bars =10 μm.

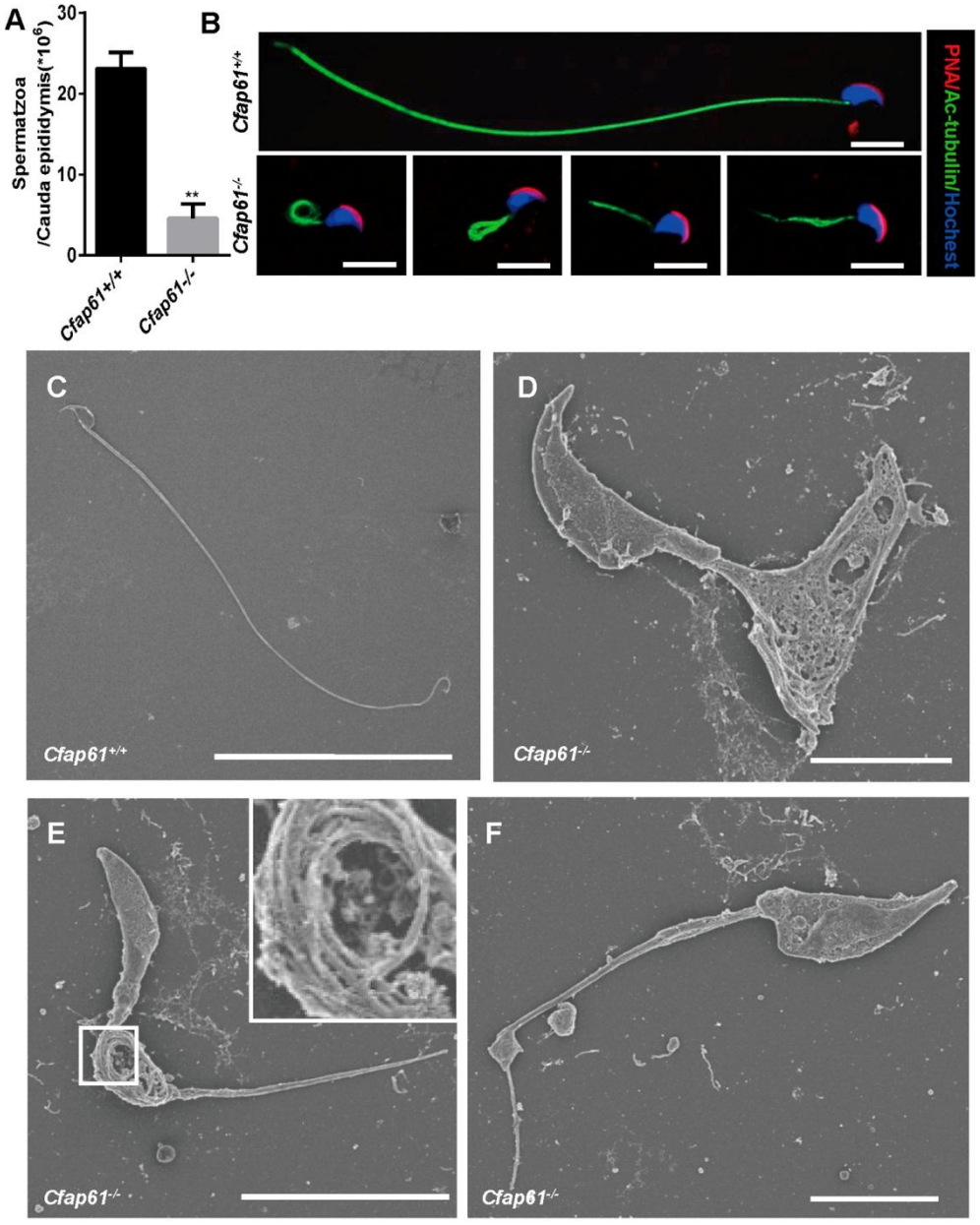

Fig. 5：Spermatozoa appear abnormal in *Cfap61*$^{-/-}$ mice.

(A) The sperm concentration of WT (23.15±1.998) and *Cfap61*$^{-/-}$ (4.593±1.760) male mice (n=3). P (*Cfap61*$^{-/-}$ vs WT)= 0.002. Data represent mean±s.e.m. (B) Fluorescence detection of Ac-tubulin (green) and PNA (red) on wild-type and *Cfap61*$^{-/-}$ spermatozoa. (B)Scale bars =10 μm.(C-F) Scanning electron micrographs of wild-type (C) and *Cfap61*-knockout (D-F) sperm. Sperm from wild-type mice show normal morphology while sperm from *Cfap61*$^{-/-}$ mice show severe flagella morphology defects. The arrangement of microtubules was reticular (D), coil like (E) and irregular (F) in different segments. The enlarged section shows coil like arrangement of microtubules (E). (C)Scale bar =50 μm.(D, F) Scale bars =5 μm.(E) Scale bar =10 μm.

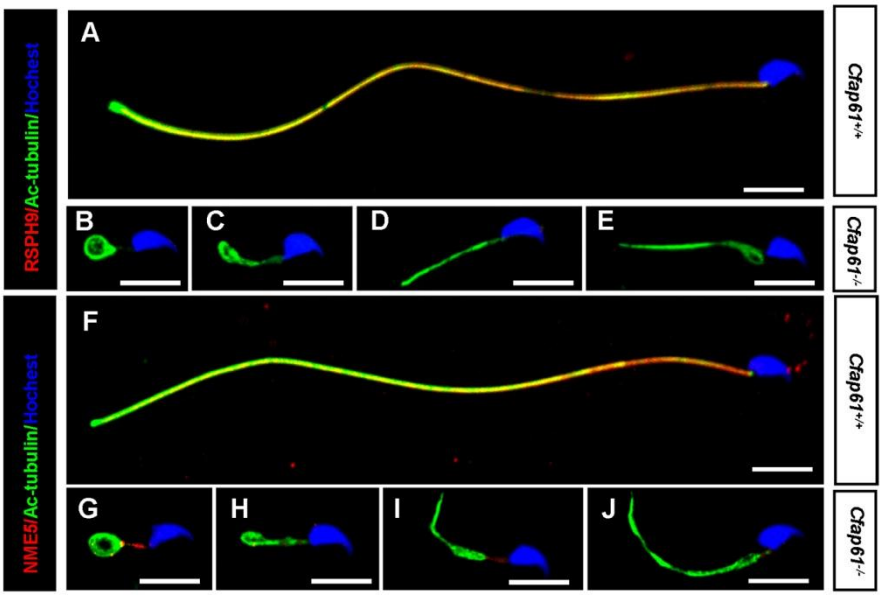

Fig. 6：Immunofluorescence analysis of radial spoke proteins in mouse sperm flagellum. (A-E) Subcellular localization of RSHP9 (red) and acetylated tubulin (green) in the sperm flagellum in wild-type (A) and *Cfap61*$^{-/-}$ mice (B-E). (F-J) Subcellular localization of NME5 (red) and acetylated tubulin (green) in the sperm flagellum in wild-type (F) and *Cfap61*$^{-/-}$ mice (G-J). Scale bars =10 μm.

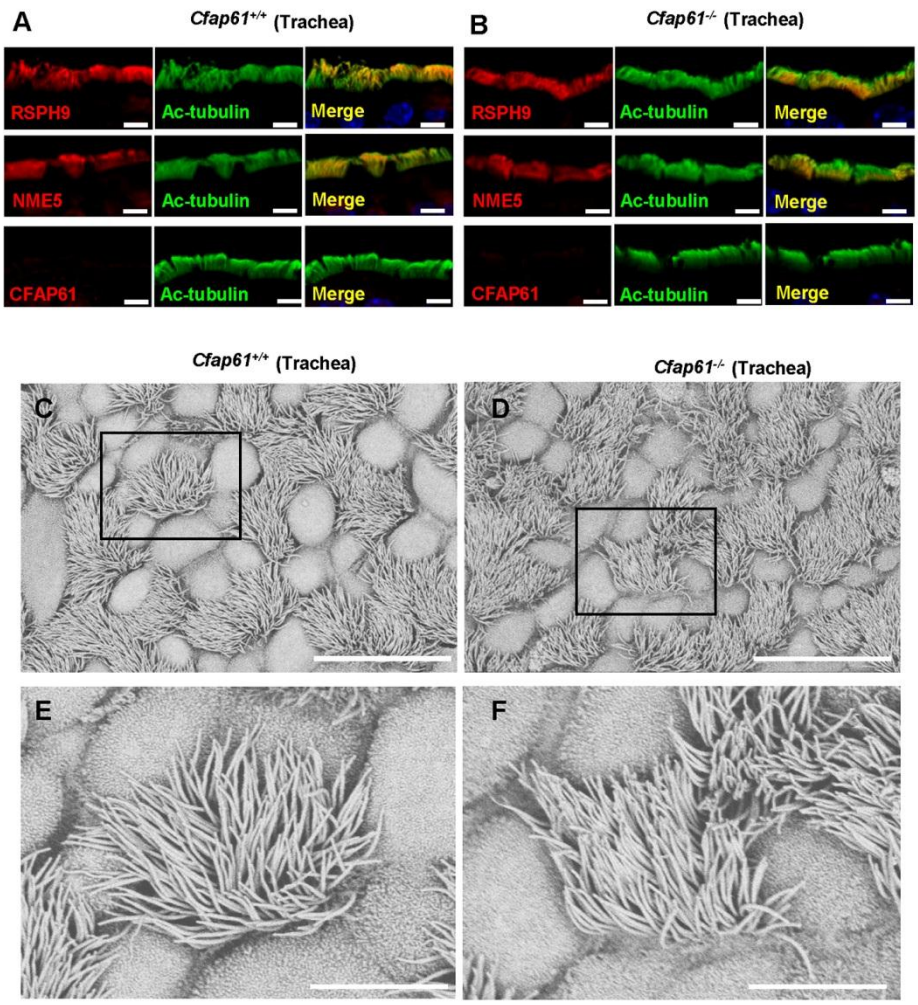

Fig. 7： Trachea cilia appear normal in *Cfap61*$^{-/-}$ mice.

(A,B) Subcellular localization of RSHP9, NME5, CFAP61 (red) and acetylated tubulin (green) in trachea cells of wild-type (A) and *Cfap61*$^{-/-}$ mice (B). (C-F) Scanning electron micrography of wild-type (C, E) and *Cfap61*$^{-/-}$ (D, F) tracheal epithelium at low (C, D) and high magnifications (E, F). (A, B) Scale bars =5 μm. (C, D) Scale bars =20 μm. (E, F) Scale bars =60 μm.

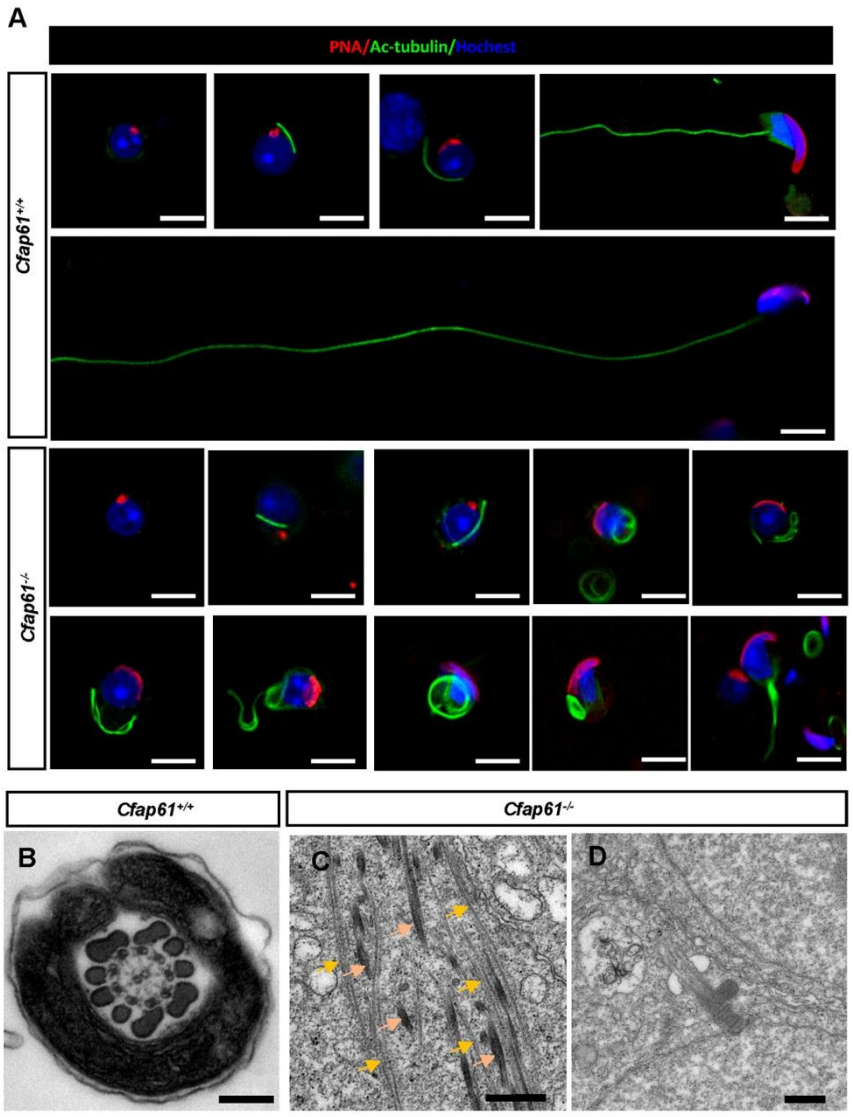

Fig. 8：Abnormal sperm flagella assembly of *Cfap61*$^{-/-}$ mice occurs from step3 round spermatids.

(A-O) Immunofluorescence analysis of acetylated-tubulin (green) and PNA (red) from wild-type (A-E) and *Cfap61*$^{-/-}$ germ cells (F-O). Ultrastructural analysis of wild-type (P) and *Cfap61*$^{-/-}$ testicular spermatozoa flagella (Q, R). (Q) The dispersed microtubules could not form "9 + 2" axonemes. The yellow arrow indicates microtubule. The pink arrow indicates the outer dense fiber. (R) The centriole of round sperm can be anchored to the nuclear membrane. (A-O) Scale bars =10 μm.(P, Q) Scale bars =200 nm.(R) Scale bar =500 nm.

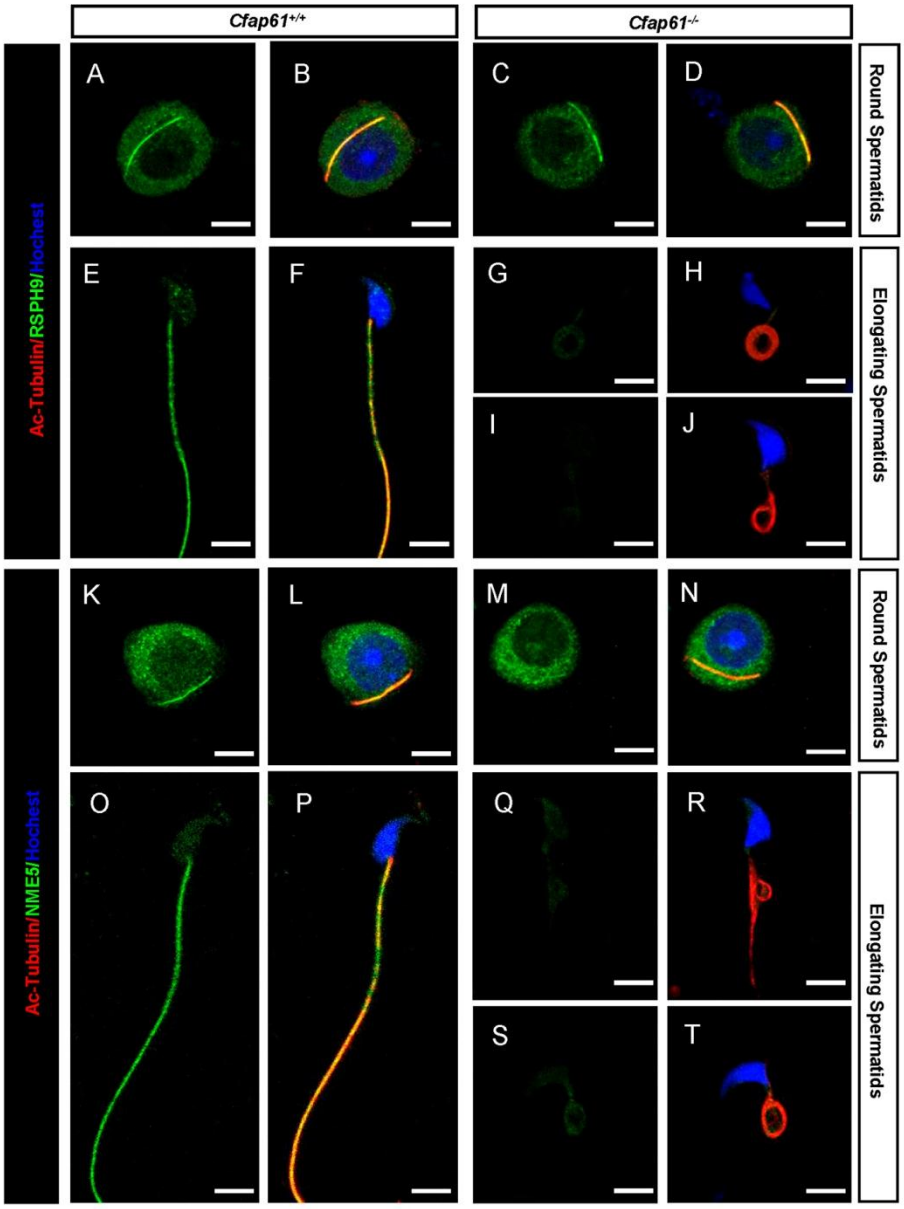

Fig. 9：Ablation of *Cfap61* affects the assembly of 20S radial spoke complex, while the 12S complex is unaffected.

(A-J) Immunofluorescence analysis of acetylated-tubulin (red) and RSPH9 (a component of the 12S radial spoke complex; green) in wild-type (A, B, E, F) and *Cfap61*$^{-/-}$ germ cells (C, D, G, H, I, J). (K-T) Immunofluorescence analysis of acetylated-tubulin (red) and NME5 (a component of the 20S radial spoke complex; green) in wild-type (K, L, O, P) and *Cfap61*$^{-/-}$ germ cells (M, N, Q, R, S, T). Scale bars =5 μm.

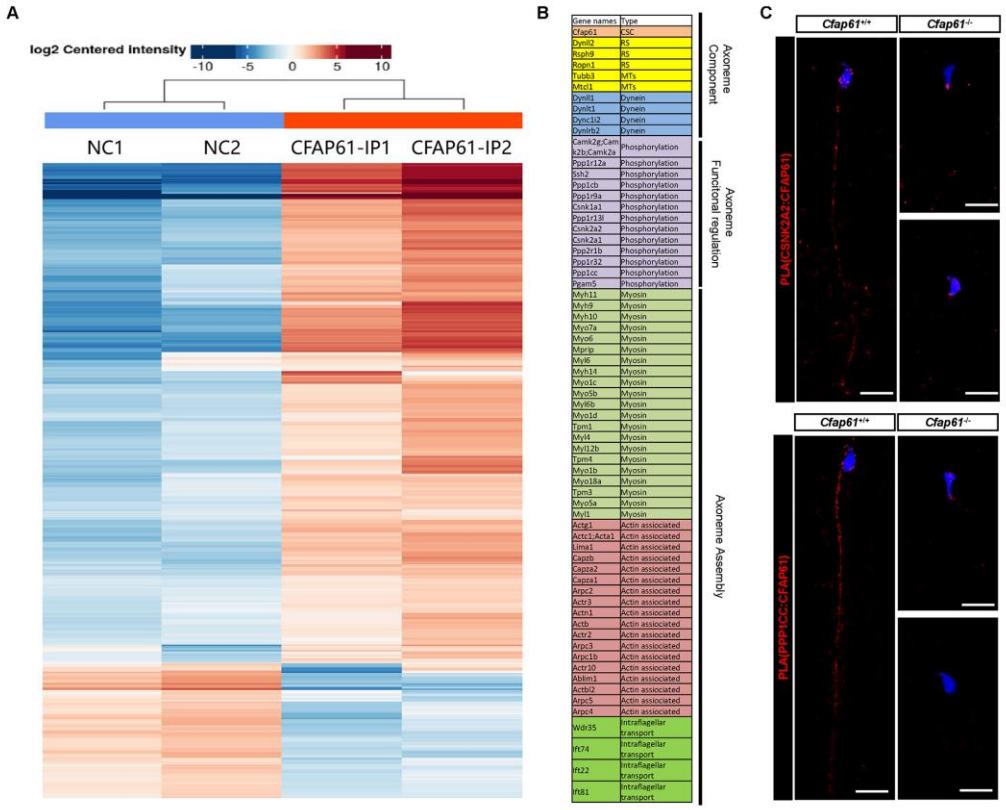

Fig. S1. Identification of CFAP61 interacting proteins.

(A) Heatmap representation of CFAP61 interacting proteins identified with anti-CFAP61. IP1-NC1 and IP2-NC2 represent data from two biological replicates. (B) Functional classes of CFAP61 interacting proteins. (C) Representative immunofluorescence image from proximity ligation assay (PLA) performed on epididymal sperm from wild-type and *Cfap61*$^{-/-}$mice. Evidence of proximity (distance < 40 nm) between CFAP61 and CSNK2A2(upper panel)/PPP1CC(lower panel) is indicated by the appearance of red dots. Nuclei were stained with DAPI (blue). Scale bars =10 μm

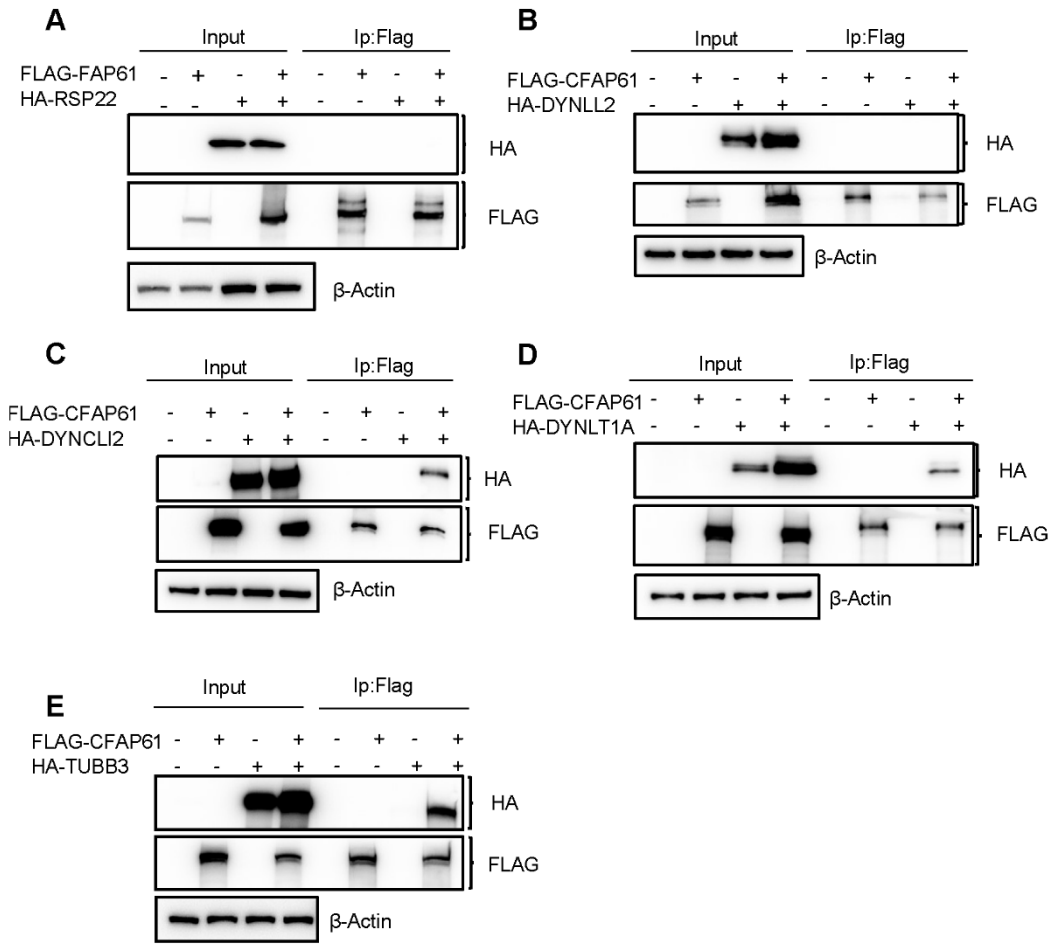

Fig. S2. CFAP61 interacts with DYNEIN and TUBULIN.

(A) Chlamydomonas RSP22 was expressed or co-expressed with FAP61 in HEK293T cells and FAP61 interaction with RSP22 was examined by co-immunoprecipitation.(B) Mouse DYNLL2(RSPH22) was expressed or co-expressed with CFAP61 in HEK293T cells and CFAP61 interaction with RSPH22 was examined by co-immunoprecipitation. (C-E) Mouse dynein subunits (C-D) or TUBB3 (E) were expressed or co-expressed with CFAP61 in HEK293T cells and CFAP61 interaction with DYNLL2, DYNCLI2, DYNLT1A, TUBB3 was examined by co-immunoprecipitation.

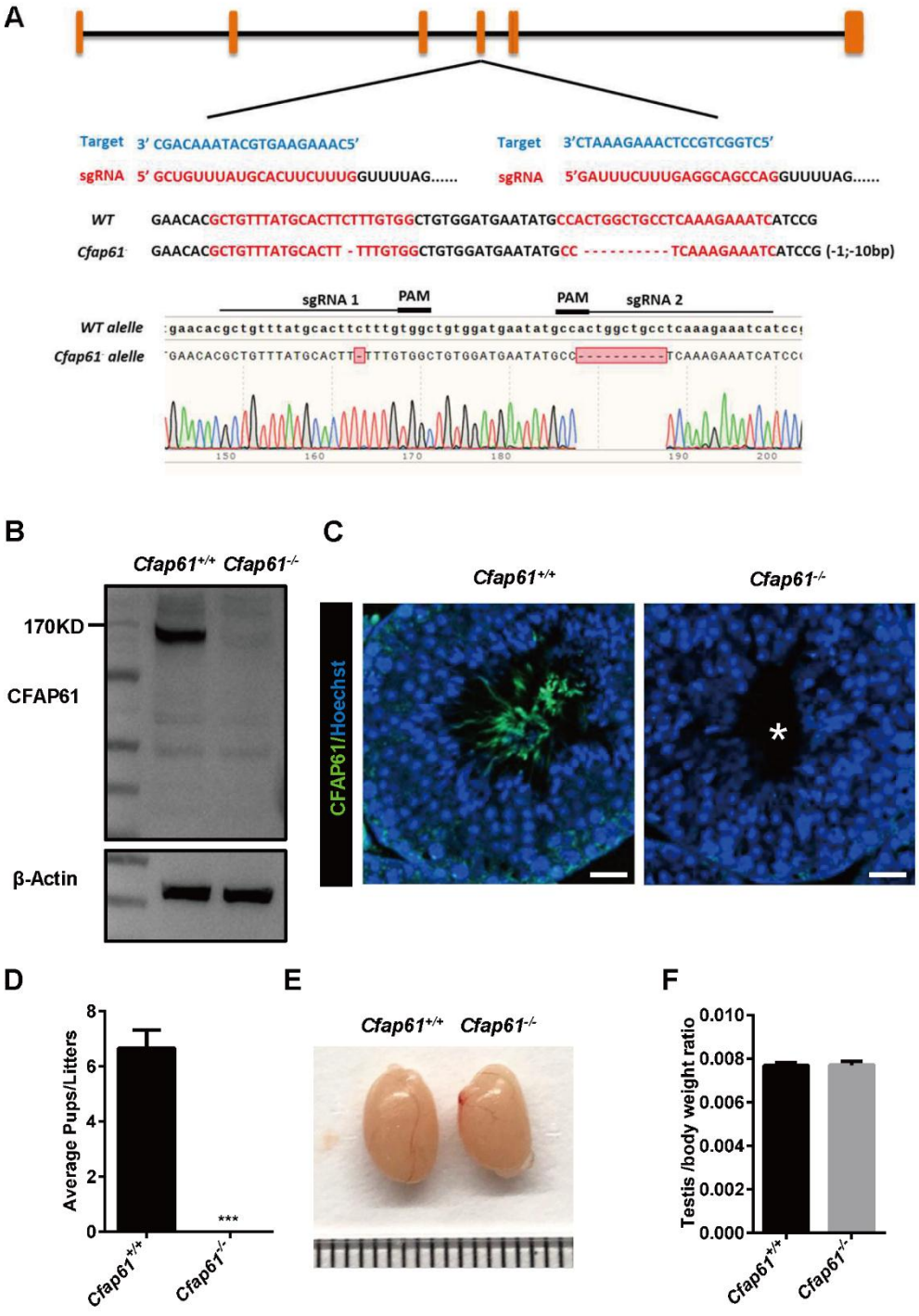

Fig. S3. *Cfap61*$^{-/-}$ mice are infertile.

(A) Schematic diagram of CRISPR/Cas9 targeting strategy. The sgRNAs were designed within exon 4 of *Cfap61* and a 1-bp and 10-bp deletion was detected in *Cfap61*$^{-/-}$ mice by Sanger sequencing. (B, C) CFAP61 was not detected in *Cfap61*$^{-/-}$

testis by western blot (B) and immunofluorescence (C). Scale bars =20 μm. (D) The average litter size of WT (6.677±0.667), *Cfap61*$^{-/-}$ (0), male mice (n=3). P (*Cfap61*$^{-/-}$ vs WT)= 0.0006. (E) The size of the testes was not altered in the WT and *Cfap61*$^{-/-}$ adult mice. (F) The testis/body weight ratio of WT (0.007689±0.0001418), *Cfap61*$^{-/-}$ (0.007721 ±0.000175) , male mice (n=3). P (*Cfap61*$^{-/-}$ vs WT)= 0.8948. Data represent mean±s.e.m.

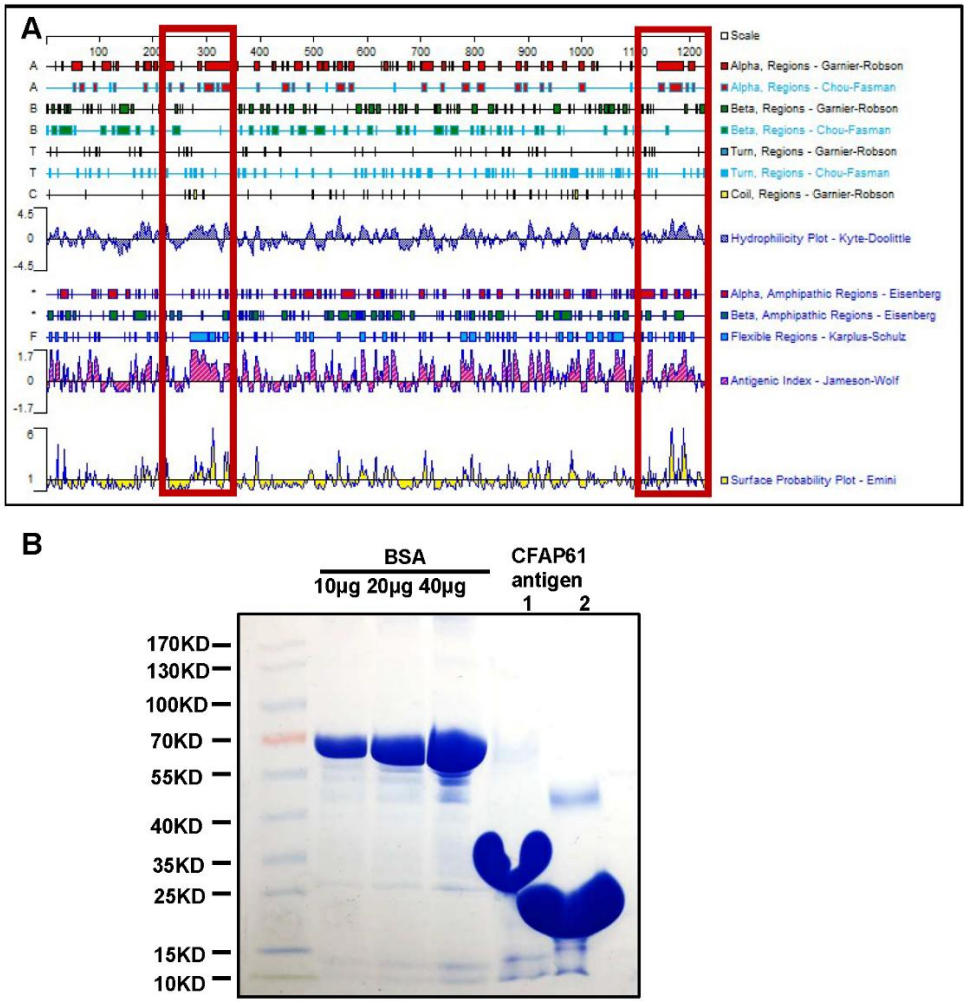

Fig. S4. Antigen selection and purification.

(A) Epitope prediction of CFAP61 by analyzing secondary structures and other indicators (flexibility, hydrophilicity, antigenicity, and surface probability). (B) Coomassie brilliant blue stained SDS-PAGE of selected antigens. Protein standards indicate molecular size in kilodaltons in leftmost lane, while next three lanes show the indicated microgram amounts of pure bovine serum albumin (BSA) and final two lanes show purified CFAP61 antigens.

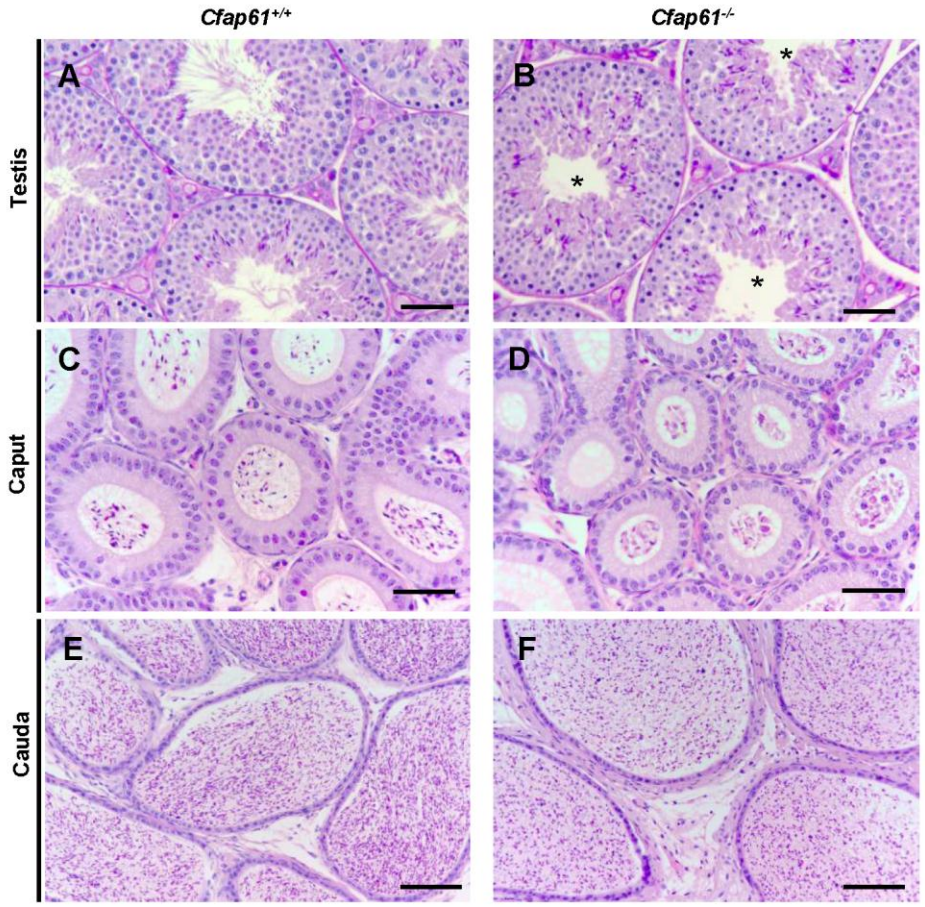

Fig. S5. Spermatogenesis is abnormal in *Cfap61*$^{-/-}$ mice.

Sections of periodic acid Schiff-stained testis and hematoxylin and eosin-stained caput and cauda epididymis from wild-type (A, C, E) and *Cfap61*$^{-/-}$ (B, D, F) mice. (A-D) Scale bars =50 μm. (E, F) Scale bars =100 μm.

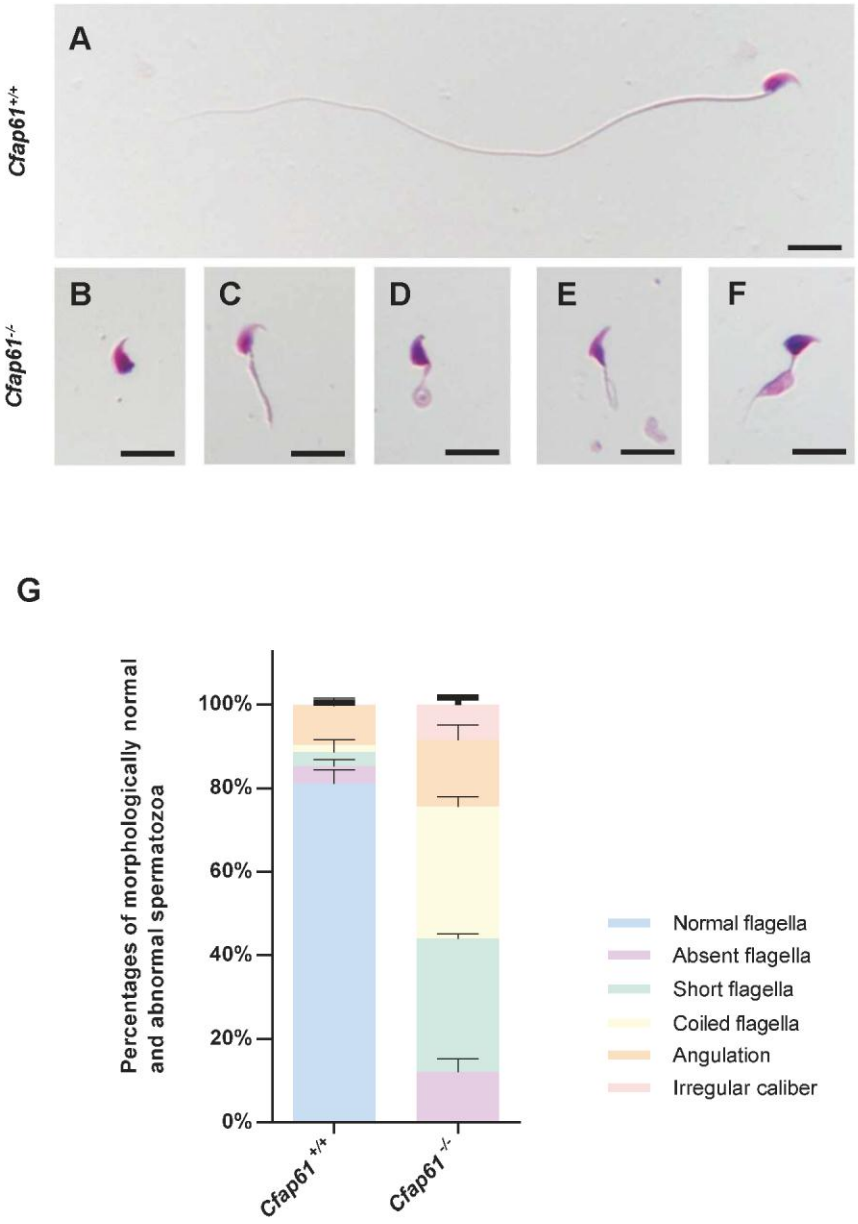

Fig. S6. Sperm morphology study in *Cfap61*$^{-/-}$ male mice.

(A) Light microscopy showed wild type spermatozoon with normal morphology while spermatozoa from *Cfap61*$^{-/-}$ mice manifested aberrant flagellar morphologies: absent (B), short (C), coiled (D), angulation (E) and irregular caliber (F), consistent with the MMAF phenotype. Scale bars =10 μm. (G) Percentage of morphologically normal

and abnormal spermatozoa in WT and *Cfap61*$^{-/-}$male mice (n=3), evaluated following the WHO guidelines. The left column shows that the percentage of spermatozoa with normal flagella(81.165±1.895%), absent flagella(4.028±0.966%), short flagella (3.414±1.709%), coiled flagella (1.604±0.783%), anjulation (9.366±1.139%) and irregular caliber (0.423±0.259%) in the normal group.The right column shows that the percentage of spermatozoa with normal flagella(0%), absent flagella(12.085±1.852%), short flagella (31.969±0.654%), coiled flagella (31.542±1.317%), anjulation (15.833±2.125%) and irregular caliber (8.570±0.940%) in the *Cfap61*$^{-/-}$ group. $P_{\text{normal flagella}}$ (*Cfap61*$^{-/-}$vsWT)= 1.77×10^-6 , $P_{\text{absent flagella}}$ (*Cfap61*$^{-/-}$vsWT)= 0.0182, $P_{\text{short flagella}}$ (*Cfap61*$^{-/-}$vsWT)= 9.84×10^-5 , $P_{\text{coiled flagella}}$ (*Cfap61*$^{-/-}$vsWT)= 4.04×10^-5, $P_{\text{angulation}}$ (*Cfap61*$^{-/-}$vsWT)= 0.055, $P_{\text{irregular caliber}}$ (*Cfap61*$^{-/-}$vsWT)= 0.001. Data represent mean±s.e.m.

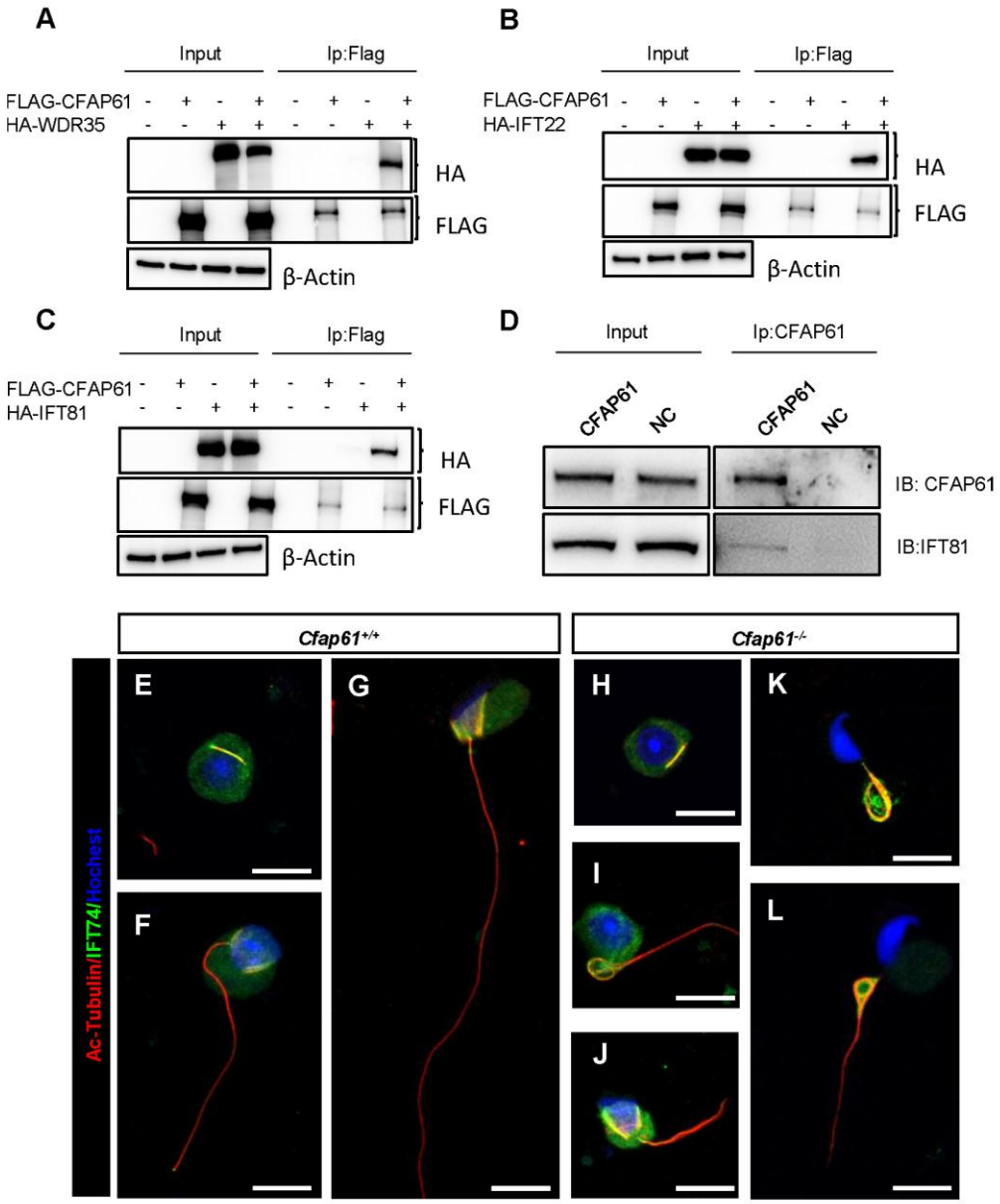

Fig. S7. Intraflagellar transport protein are retained in mature spermatozoa .

(A-C) Intraflagellar transport (IFT) proteins were expressed or co-expressed with CFAP61 in HEK293T cells, and CFAP61 interaction with IFT proteins was examined by co-immunoprecipitation. (D) Co-IP analysis of CFAP61 and IFT81 from testicular protein extracts. (E-L) Immunofluorescence analysis of acetylated-tubulin (red) and IFT74 (green) in wild-type (E-G) and *Cfap61*$^{-/-}$ germ cells (H-L). Scale bars =10 μm.

Table S1. Primer sequences For qRT-PCR

Primer	Sequence
Cfap61-qRT-F	TCCCATGCACACCTCTGAAC
Cfap61-qRT-R	AAGTACAGTTCTGGCACCGC
Wdr66-qRT-F	AAGCTCCTCCCTGGCTGATA
Wdr66-qRT-R	TGTCTTCAGGCTTCTGGCTG
Maats1-qRT-F	CAGCACCATGAGCCAGACAG
Maats1-qRT-R	ACACAATAAATAACGGGTCGTACA
Rsph9-qRT-F	ATGACATCCCCAGAGGGTCT
Rsph9-qRT-R	GGAGCGTGGTAGAAGGTGAG
Ropn1l-qRT-F	TCCTGCACAAGCAGTGTAGC
Ropn1l-qRT-R	TCCAGCTCCAGGATCGTTCT
Rsph4a-qRT-F	TGGTCGAGACAGCTATGAGGA
Rsph4a-qRT-R	ACCAATTACAGCGACCCTGAG
18s-F	TAACGAACGAGACTCTGGCAT
18s-R	CGGACATCTAAGGGCATCACAG

Table S2. Primer sequences For plasmids construction

Primer	Sequence
Flag-Cfap61-F	AAGGATGACGATGACAAGCTTTCCATCCTCACGTCCCCCAG
Flag-Cfap61-R	CCACACTGGACTAGTGGATCCCTAAATGATGCCTGGCCATGCG
HA-Armc4-F	TACGCATCAGCGGAAAAGCTTGGTGTGGCGTTGACCAGGTTG
HA-Armc4-R	CCACACTGGACTAGTGGATCCTCAGTTGTATCTAGCCTTTTCTGTAGCAAGAG
HA-Calm4-F	TACGCATCAGCGGAAAAGCTTTCTCACGGGTTTACTAAGGAGGAGGTC

HA-Calm4-R	CCACACTGGACTAGTGGATCCTCAATTTTCAACGTGGAGGCGC
HA-Maats1-F	TACGCATCAGCGGAAAAGCTTAGCCAGACAGTGACCATCCAGGAA
HA-Maats1-R	CCACACTGGACTAGTGGATCCCTAGCCTTCTCCCTCATCCTGAGTAGG
HA-Rsph3a-F	TACGCATCAGCGGAAAAGCTTGCCGCCACCAACATTTGGG
HA-Rsph3a-R	CCACACTGGACTAGTGGATCCTCACTCTGCCATAAGGTGTCCCC
HA-Dynll2-F	TACGCATCAGCGGAAAAGCTTTCTGACCGGAAGGCAGTGATCAA
HA-Dynll2-R	CCACACTGGACTAGTGGATCCCTAGCCCGACTTGAAGAGGAGGATT
HA-Ropn1-F	TACGCATCAGCGGAAAAGCTTCCTCAGACAGACAAGCAAGTATGC
HA-Ropn1-R	CCACACTGGACTAGTGGATCCTTATTCCAGCCGAACCCTAGGGT
HA-Ropn1l-F	TACGCATCAGCGGAAAAGCTTCCGCTGCCCGACACCA
HA-Ropn1l-R	CCACACTGGACTAGTGGATCCCTATATTATCTTTTTTCCAACGAAGAAGTCCGAAAGT
HA-Rsph9-F	TACGCATCAGCGGAAAAGCTTGACGCCGACAGCCTCTTG
HA-Rsph9-R	CCACACTGGACTAGTGGATCCCTACAGCATGAAGGGCAAGTCCA
HA-Wdr35-F	TACGCATCAGCGGAAAAGCTTTTCTTCTACCTGAGCAAGAAAATTGCTGT
HA-Wdr35-R	CCACACTGGACTAGTGGATCCTTATTCTACCGAGCTGTGGCATAAAGG
HA-Ift22-F	TACGCATCAGCGGAAAAGCTTCTGAAGGCTAAGATCCTCTTCGTGGG
HA-Ift22-R	CCACACTGGACTAGTGGATCCCTAGGTGATGATGAGCATCTCCTCGC
HA-Ift74-F	TACGCATCAGCGGAAAAGCTTGCCAGTAATCACAAATCTTCAGCCC
HA-Ift74-R	CCACACTGGACTAGTGGATCCTCAGCTTCTGCTGGCATTATGTAGAGC
HA-Ift81-F	TACGCATCAGCGGAAAAGCTTAGTGACCAAATCAAATTCATCGTGGAC
HA-Ift81-R	CCACACTGGACTAGTGGATCCTCAGAGAACCAGCCGGTCCTCTC
HA-Dyncli2-F	TACGCATCAGCGGAAAAGCTTTCGGACAAAAGTGATTTAAAAGCTGAGTT

HA-Dyncli2-R	CCACACTGGACTAGTGGATCCCTAGGCAGGGATTCGGGTAGCTG
HA-Dynll1-F	TACGCATCAGCGGAAAAGCTTTGCGACCGGAAGGCGGT
HA-Dynll1-R	CCACACTGGACTAGTGGATCCTTAACCAGATTTGAACAGAAGAATGGCC
HA-Dynlrb2-F	TACGCATCAGCGGAAAAGCTTACAGAAGTGGAGGAAACCCTCAAGAG
HA-Dynlrb2-R	CCACACTGGACTAGTGGATCCCTACTCACATGGGTTCTGAATGACAATCA
HA-Dynlt1a-F	TACGCATCAGCGGAAAAGCTTGAAGACTTCCAGGCCTCCGAGG
HA-Dynlt1a-R	CCACACTGGACTAGTGGATCCTCAGATGGACAGTCCGAAGGTACTGA
exon1-F	TTTGGCAAATCTAGAGGATCCAGGCTGCGCGTCCTCCTTG
exon1-R	AGGAGCAGAGCTTACCTCATCCGCAGCTCCAGGAC
intron1'+exon2+intron2'-F	GTAAGCTCTGCTCCTGAATTAATTCTATCCC
intron1'+exon2+intron2'-R	AGGTTGGCCTTTTCTCTGCCAGGGAGGTCATGTCA
exon3-33-F	AGAAAAGGCCAACCTTGCTGTTAC
exon3-33-R	GTAGTCCATGTCGACAAGCTTAACGATGCCTGGCCACGC
firely luciferase-F	ATTGGGTACCTTAATAAATGAGTCTTCGGACCTCGC
firely luciferase-R	ATCCCTCGACTTAATTACCACATTTGTAGAGGTTTTACTTGCTTTAAAAAAC

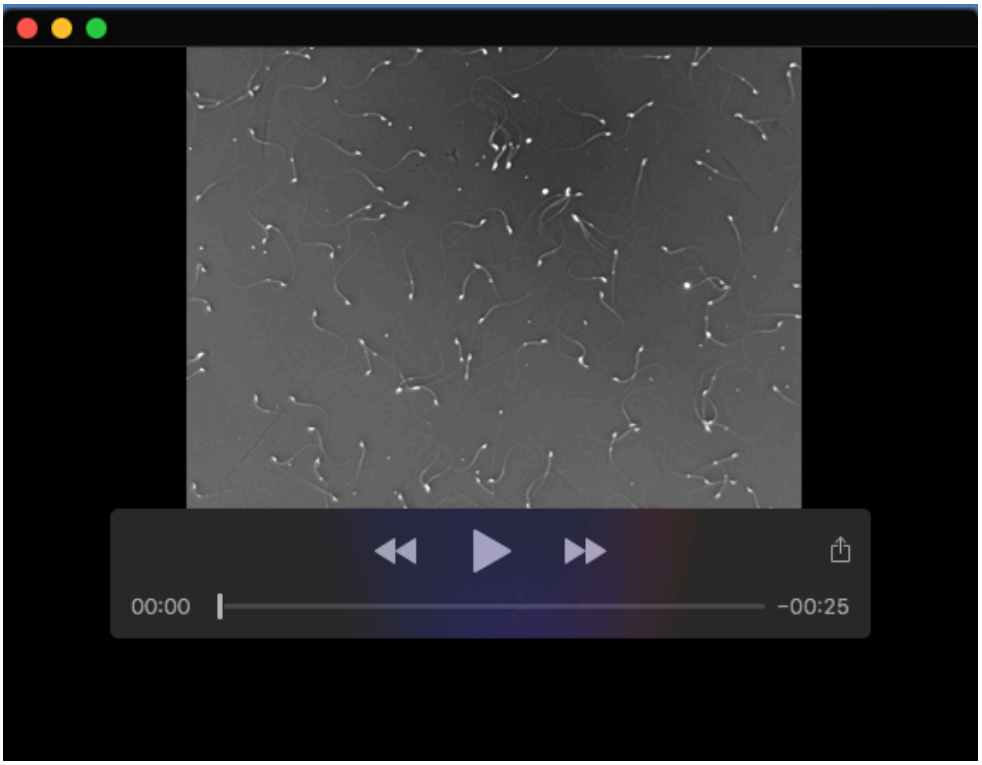

Movie 1. Motility and movement of the sperm from the caput epididymis of wild-type male mice.

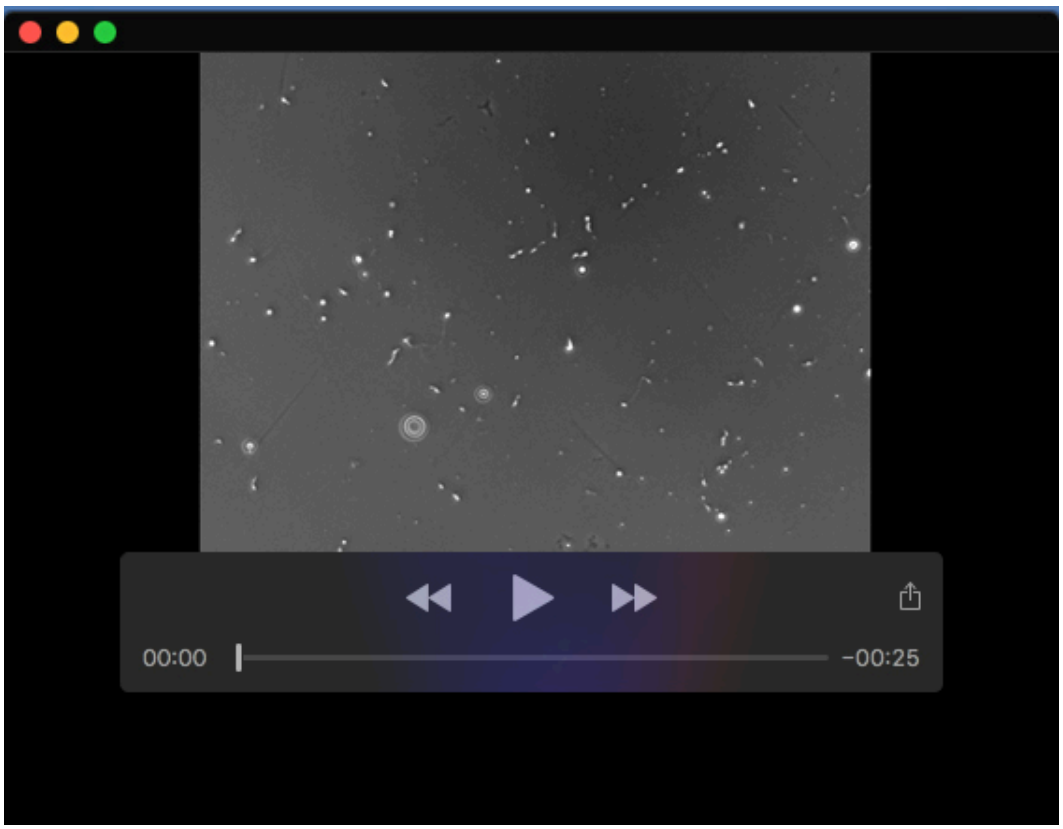

Movie 2. Motility and movement of the sperm from the caput epididymis of *Cfap61*$^{-/-}$ male mice.

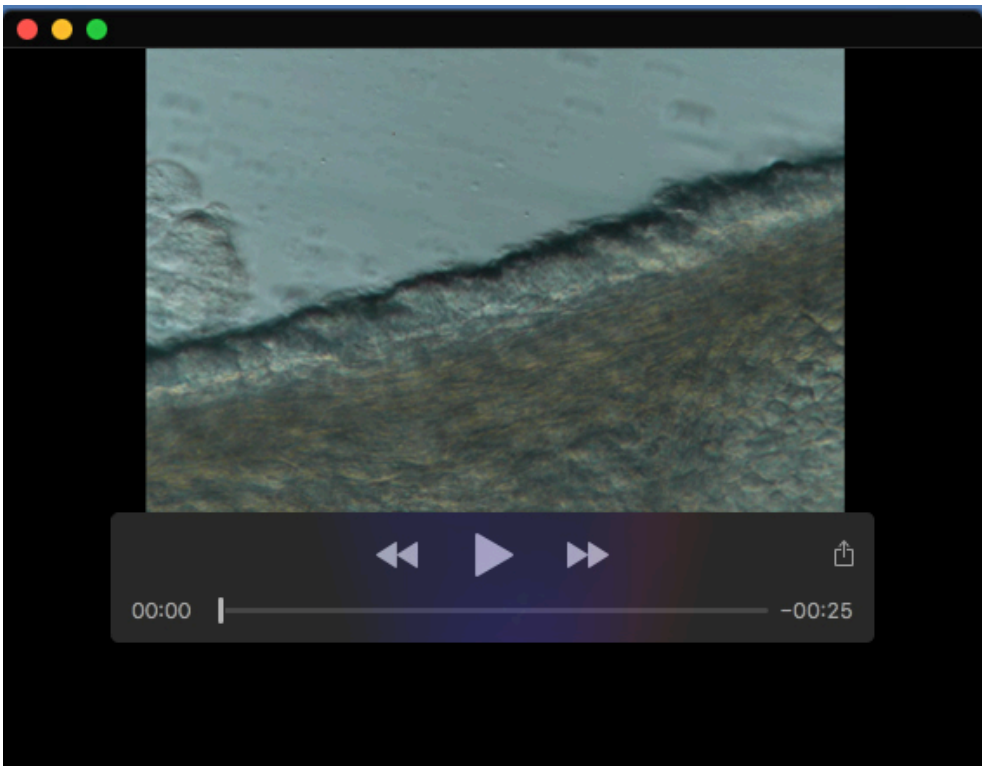

Movie 3. Ciliary motility of wild type tracheal epithelial cells.

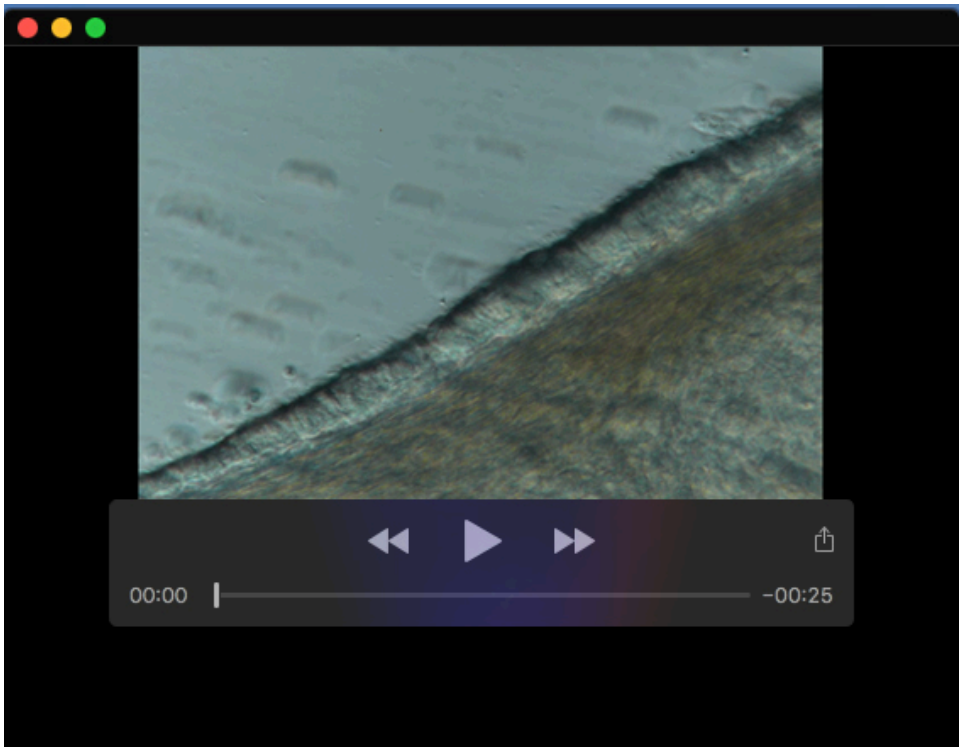

Movie 4. Ciliary motility of *Cfap61*$^{-/-}$ tracheal epithelial cells.